Chapter 15

Microstructural Characteristics and Mechanical Behaviors of New Type SIMA Processed Aluminum Alloy

Chia-Wei Lin, Fei-Yi Hung and Truan-Sheng Lui

Additional information is available at the end of the chapter

http://dx.doi.org/10.5772/intechopen.70462

Abstract

In this chapter, a new type strain-induced melt activation (SIMA) process for Al-Mg-Si alloys was used. The microstructural characteristics, formability at elevated temperature and mechanical properties were estimated. The high-hardness globular grain boundaries are formed by eutectic phases. This new type SIMA process has proved that it can decrease high temperature compression resistance and improve ability of metal flowing at high temperature. After SIMA forming process, the mechanical properties of materials can be improved via artificial aging and can be competed with general artificial aged materials. All results show that this SIMA process is a potential process.

Keywords: strain-induced melt activation, microstructural evolution, high temperature formability, mechanical properties, erosion resistance

1. Introduction

1.1. Strain-induced melt activation (SIMA) process

Semi-solid metal forming process is a hybrid net shape process that combines the advantages of forging and casting [1, 2]. Materials are manufactured at the temperature of solid-liquid coexistence and perform good high temperature formability [3–5]. Magneto-hydrodynamic (MHD) stirring casting, spray casting and strain-induced melting activation (SIMA) are three common semi-solid process for getting fine and globular grains that can enhance formability at elevated temperatures [6, 7].

The SIMA process is useful because of its low cost, simple equipment and high stability. **Figure 1(a)** reveals steps of the traditional SIMA process [8]. Casting, hot work, cold work and heat treatment for partial melting and grain spheroidization are four major steps of traditional SIMA process. A promoted and new type of SIMA process is proposed here. The two main dissimilarities between two SIMA processes are: (1) this new process uses severe hot extrusion instead of cold work to introduce sufficient amount of strain energy and (2) the new process uses a salt bath for heating to enhance heating uniformity and to reduce heating duration. **Figure 1(b)** shows the steps of this process.

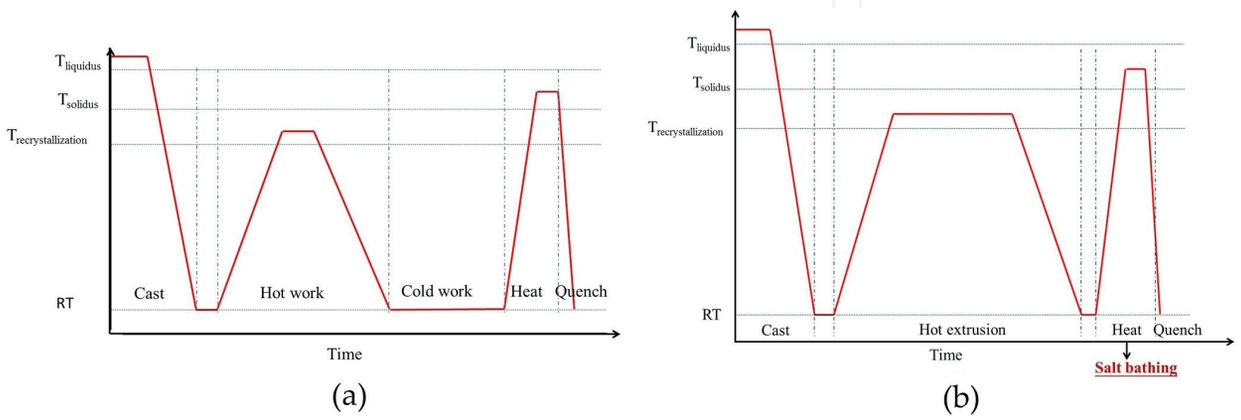

Figure 1. Procedures of (a) traditional strain-induced melt activation (SIMA) process and (b) new type SIMA process. RT, room temperature.

The mechanisms of globular grain formation for the traditional SIMA [8, 9] process are shown in **Figure 2**. The procedures are: (1) casting; (2) hot work for disintegrating the casting structure; (3) cold work for introducing sufficient strain energy; and (4) heat treatment for making alloys recrystallize and partially melt at the temperature of muzzy zone. In the step of heat treatment, grains recrystallize and phases with low melting point and parts of eutectic composition start to melt partially and penetrate to the grain boundaries of recrystallized grains due to their high free energy. It results in liquid phases surrounding the fine recrystallized grains. Finally, grain growth occurs and generates spheroidized grains as heating carry on because the surface energy of global grains is the smallest.

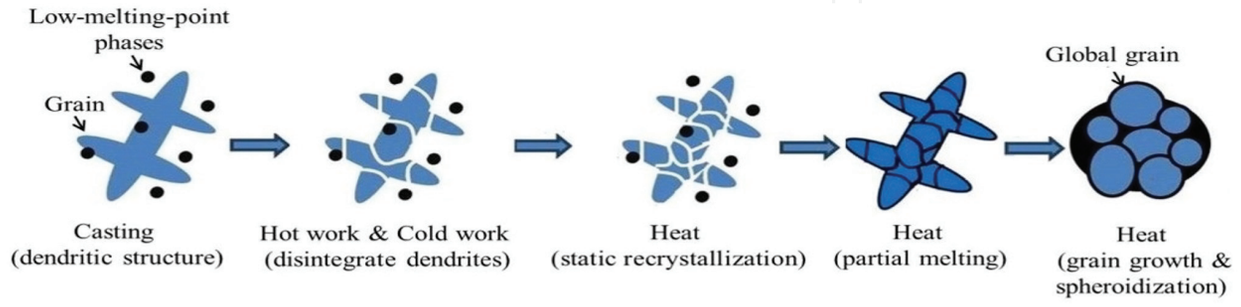

Figure 2. Evolution of globular grain formation in traditional SIMA process.

For the growth mechanism of globular grains, when alloys are heated to the temperature of solid-liquid coexistence, two coarsening mechanisms are considered [7, 10–13]: grain coalescence and Ostwald ripening. Ostwald ripening dominates for higher liquid fractions and long-duration heating, and grain coalescence dominates for lower liquid fractions and short-duration heating. In general, Oswald ripening should be the major growth mechanism of globular grains. The globular grain growth is based on Lifshitz-Slyozov-Wagner (LSW) theory [1, 14–18]. The formula is $d^n - d_0^n = Kt$, where d is the average globule size that depends on salt bath duration, d_0 is the initial globule size, t is the duration of salt bath, K (units: $\mu m^3\ min^{-1}$) is the coarsening rate constant and exponent n is determined by the diffusion mechanism of grain growth. Ostwald ripening is the major mechanism of globular grain growth of SIMA alloys in the case of liquid fraction being sufficient [10–13]. As $n = 3$, the mechanism of grain growth is Ostwald ripening. The theoretical formula can be rewritten as $d^3 = Kt + d_0^3$. Ostwald ripening is a dissolution-precipitation diffusion-controlled mechanism [10–13]. Large grains become larger and small grains become smaller and even disappear.

1.2. 6xxx aluminum alloys

6xxx Al alloys, a series of precipitation-hardened Al alloys [19], are widely used. More than 70% of extruded Al alloys are 6xxx Al alloys, therefore, this series alloy is chosen for this chapter of new type SIMA process, as hot extrusion is a major step in this process. Similar results and discoveries can be seen in other series of aluminum alloys.

The major components of 6xxx series aluminum alloys are Mg and Si. The Mg_2Si phase is generated first since its forming free energy is lower than those of other precipitating phases [20–22]. 6xxx aluminum alloys with more Si that are required to form stoichiometric Mg_2Si commonly have relatively high strength and low ductility due to the hard and brittle Si particles in their matrix. In contrast, 6xxx aluminum alloys with excess Mg have relatively low strength and high ductility. Besides Mg and Si, Cu, Mn, Cr, Zr, Sc and V are added to these alloys. Adding Mn inhibits grain growth, enhances strength, and increases recrystallization temperature [20, 23, 24]. Adding Cu improves strength and hardness due to the refining of the precipitated phase during artificial aging [13–16]. Adding Cr promotes corrosion resistance [23]. Adding Zr enhances strength since Al_3Zr is generated and grain growth is inhibited, and adding Sc or V retards grain growth [24, 25].

1.3. Topics of this study

In short, 6xxx Al-Mg-Si alloys are the major materials for the new type SIMA process. There are three essential topics to be exhibited: (1) microstructural characteristics and microstructure evolution of SIMA processed Al-Mg-Si alloys and their relationship with parameters of SIMA process; (2) formability and deformation mechanism at elevated temperatures of SIMA-processed Al-Mg-Si alloys and (3) the mechanical properties improvement of SIMA forming alloys and its strengthening mechanism. These above topics are discussed in following sections in sequence.

2. Microstructure evolution and microstructural characteristics of new type SIMA-processed alloys

2.1. Brief introduction

The degree of spheroidization and globule size affect high temperature formability obviously in SIMA process [3–5]. Highly spheroidized, fine and uniform globules lead to high formability at elevated temperatures. Hence, how to control hot extrusion conditions, how to design proper material composition and how to determine parameters of SIMA process to get fine, uniform and highly spheroidized globule is the major theme of discussion in this section.

Seven kinds of hot-extruded Al-Mg-Si alloys with different composition or fabricated by distinct extrusive ratio were used for discussing the effects of composition and extrusive ratio. The target is to build a principle for designing suitable materials for new type SIMA process and to choose most proper alloy for further researches [26].

2.2. Experimental methods

2.2.1. Designing and choosing alloys

The compositions and codes of seven kinds of Al-Mg-Si alloys are shown in **Table 1**. All the materials are extruded sheet except for 6069-rod is an extruded rod. They were used for determining the influences of extrusion conditions and understanding how to design composition of alloys for SIMA process by observing their microstructure evolution.

2.2.2. New type strain-induced melt activation (SIMA) process

The flow of new type SIMA process is shown in **Figure 1(b)**. The considerable three parameters of new type SIMA process are extrusive ratio (it also means the introduced strain energy), temperature of salt bath and duration of salt bath in sequence of its flowchart. The temperatures of salt bath are set as 570–630°C due to partial melting starting at about 570°C and severe deformation occurring above 630°C in Al-Mg-Si alloys. The durations of salt bath are set from 1 to 60 min for understanding the effect of salt bath duration on globule size and degree of spheroidization.

Material	Mg	Si	Cu	Mn	Fe	Cr	V	Zr	Al
6061	0.88	0.67	0.16	0.03	0.19	0.04	0	0	Bal.
6061-Mn	0.83	0.75	0.20	0.31	0.19	0.07	0	0	Bal.
6066_3 mm	1.02	1.29	0.95	1.02	0.19	0.18	0	0	Bal.
6066_9 mm	1.02	1.29	0.95	1.02	0.19	0.18	0	0	Bal.
6069-sheet	1.25	0.75	0.73	0.05	0.13	0.16	0	0.11	Bal.
6069-rod	1.30	0.85	0.72	0.09	0.13	0.14	0.12	0	Bal.
6082	0.71	1.10	0.06	0.71	0.19	0.23	0	0	Bal.

Unit: wt.%.

Table 1. Compositions of several Al-Mg-Si alloys used in this research.

http://dx.doi.org/10.5772/intechopen.70462

The codes of salt bath specimens are interpreted by the following example: SB620-10 means a material which was heated by salt bath at 620°C for 10 min.

2.2.3. Microstructure analysis and globule size measuring

The microstructure evolution and globule size were investigated using optical microscopy (OM). The concept of an equivalent circle is used in this study. When the shape of a grain is not circular in a two-dimensional plane, grain size is represented by the diameter of the equivalent circle, as shown in **Figure 3**. Two shape parameters, x and z, were defined for the degree of spheroidization [4]. In **Figure 3**, a, b, c and A represent the major axis, minor axis, perimeter, and area of a grain, respectively. According to the definitions $x = (b/a)$ and $z = (4\pi A)/c^2$, x is the ratio of the minor axis to the major axis and z becomes closer to 1 as the shape becomes more circular. As x and z become closer to 1, the grains become more equiaxial and the degree of spheroidization increases.

In salt bath step of new type SIMA process, low melting point second phases and part of matrix with high dislocation density were partially melted at the temperature of solid-liquid coexistence, liquid generated and penetrated into recrystallized grain boundaries. It is defined as liquid phase. The fraction of liquid phases was measured using Image J software. High liquid fraction results in improvement of high temperature formability according to Refs. [3, 6, 7].

2.2.4. Elements distribution analysis and phases identification

In order to estimate the distribution of elements and phases, energy dispersive spectroscopy (EDS) integrated in scanning electron microscope (SEM) and electron probe X-ray micro-analyzer (EPMA) were used. The evolution of elements distribution and diffusion can be semi-quantified by these two instruments.

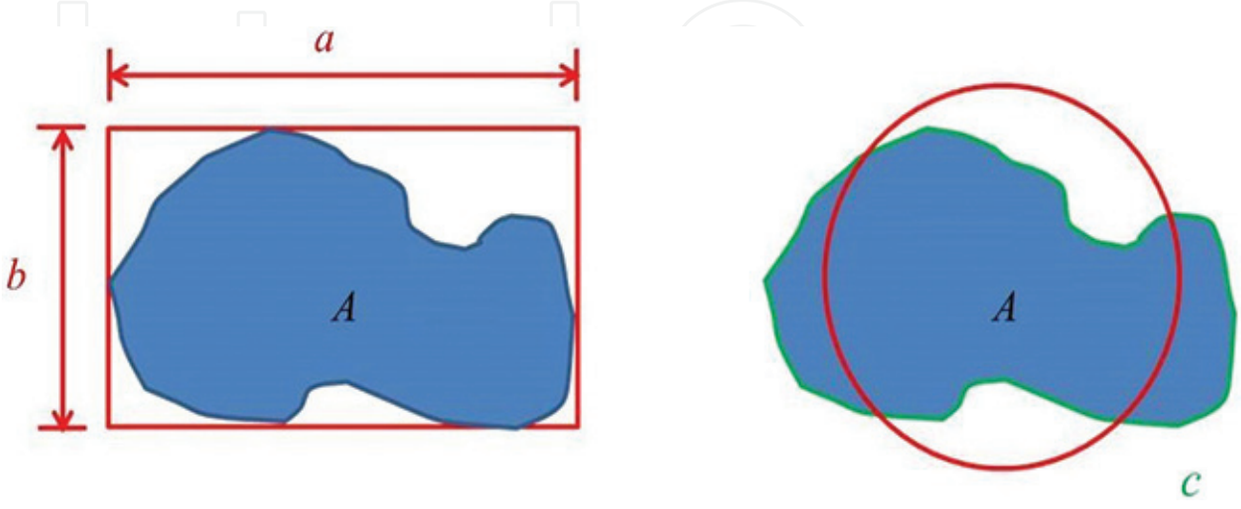

Figure 3. Parameter of spheroidization degree definition. a, b, c and A represent the major axis, minor axis, perimeter and area of a grain, respectively.

2.3. Effects of extrusive condition and chemical composition on microstructure evolution of SIMA-processed Al-Mg-Si alloys

The microstructures of the initial extruded alloys are shown in **Figure 4**. Their initial grain sizes are shown in **Table 2**. Even though the extrusion ratios of 6061 and 6061-Mn are identical, the initial grain size of 6061 is larger than that of 6061-Mn due to Mn retarding grain growth.

As the extrusion ratio increased, the level of dynamic recrystallization also increased. This can be shown by comparing the microstructures of 6066_3 mm and 6066_9 mm. The higher level of recrystallization of 6066_3 mm led to a more uniform and smaller initial grain size. Dynamic recrystallization in 6061 alloys is easier than that in 6066 alloys due to Mn addition, which increases recrystallization temperature, in the latter.

Both coarse and fine grains can be seen in 3 mm-thick 6069-sheet alloys. According to the grain coalescence mechanism, if the crystal orientations of neighboring grains are similar, the grains will easily merge, forming coarse grains. This led to the nonuniform grain distribution in 6069-sheet. In the 28 mm-diameter 6069-rod alloy, fine grains appear in the center and coarse and fine grains appear at the edge. This is due to the lower strain in the center of the rod creating a smaller driving force for grain growth, and the higher strain at the edge of the rod making some crystals with similar orientations grow and then merge. Although 6069-sheet and 6069-rod did not contain Mn, the level of grain growth of 6069 alloys was lower than that of 6061 alloys due to the addition of V and Zr.

Equiaxial grains resulted from dynamic recrystallization in the 3 mm-thick 6082 alloy due to Mn content. This confirms that Mn inhibits grain growth.

The microstructural evolution in the salt bath step for all alloys is shown in **Figure 5**. The codes of specimens subjected to a salt bath are marked with the prefix "SB." After the salt bath, grains were spheroidized and grain boundaries were broadened due to the low melting point phases melting and penetrating the grain boundaries. With grain growth, melting phases aggregated to form liquid pools [3, 4]. The alloys with spheroidized grains are defined as SIMA alloys. **Table 2** shows the liquid fraction of all alloys after a salt bath at 620°C for 10 min. Fine grains, high spheroidization degree and high liquid fraction are the major factors for promoting high temperature formability [7–9].

It is assumed that all grain growth mechanism of all materials is Oswald ripening for comparing the grain growth rate. The grain growth rate of all materials is shown in **Table 2**. This table shows that the grain growth rate of 6061-Mn is lower than 6061, and the grain growth of 6066 alloys and 6082 alloys are relatively lower than other alloys. It proves that adding Mn can decrease the rate of globular grain growth. Besides, after the salt bath, the grain size of 6066-3 mm is smaller than that of 6066-9 mm even though their grain growth rates K are almost identical. It indicates finer and more uniform dynamic recrystallized grains are beneficial for getting smaller and more uniform spheroidized grains.

Table 2 also shows the liquid fractions of the four kinds of aluminum alloy during the 10-min salt bath. The order of liquid fractions is those for 6066, 6069, 6082 and 6061 (from high to low). The liquid fractions of a given alloy are similar, except for 6061. In general, the liquid fractions

http://dx.doi.org/10.5772/intechopen.70462

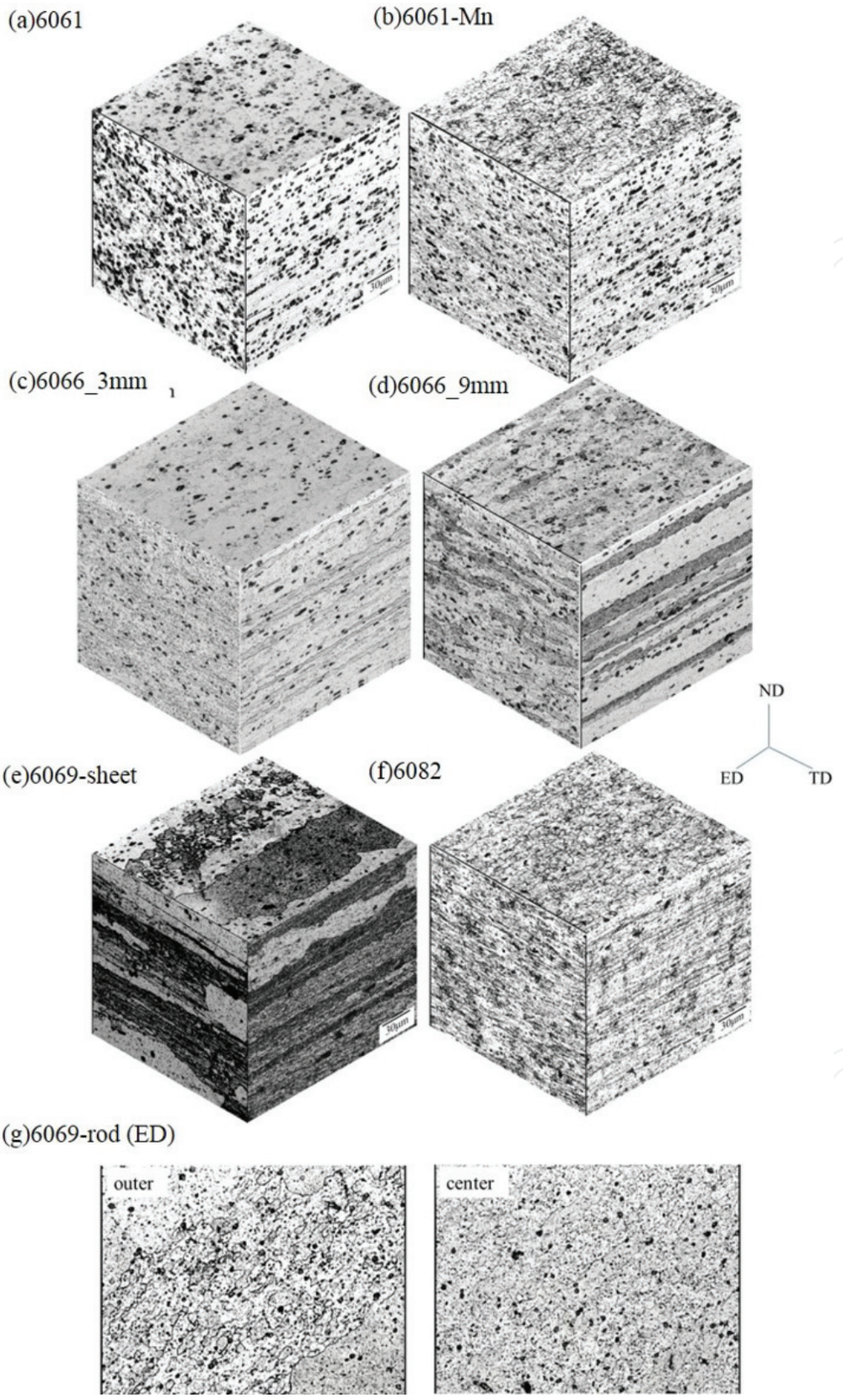

Figure 4. Microstructures of extruded Al-Mg-Si alloys: (a) 6061, (b) 6061-Mn, (c) 6066_3 mm, (d) 6066_9 mm, (e) 6069-sheet, (f) 6082 and (g) 6069-rod.

Material	Initial grain size (μm)	Liquid fraction (%) at 10 min salt bath	K ($\mu m^3\ min^{-1}$)
6061	40	3.2	42,329
6061-Mn	7	7.2	30,054
6066_3 mm	3–5	16	16,806
6066_9 mm	5–7	15.5	17,024
6069-sheet	7; 300	10.4	31,579
6069-rod (center)	15	11.2	32,678
6082	8	7.5	24,357

Table 2. Grain size, liquid fraction and growth rate of Al-Si-Mg alloys.

of a given alloy should be similar. However, the high grain growth and low liquid fraction of 6061 alloys led to position affecting the results.

The degrees of spheroidization of all alloys are shown **Figure 5**. The degrees of spheroidization of 6066 alloys and 6069-rod are higher than those of other samples. The degrees of spheroidization of 6066-3 mm, 6066-9 mm, and 6069-rod are higher due to their fine and uniform initial recrystallized grains and high liquid fraction.

The elemental distributions obtained using EPMA are shown in **Figure 6**. Mg, Si and Cu are the major elements located at grain boundaries, and Fe, Mn, Cr and V exist in the particle phases. It indicates that the melting phases in the salt bath step are mostly composed of Mg, Si, Cu and Al. The three phase diagrams in **Figure 7** show that the eutectic points of Al and Si, Al and Mg_2Si and Al and Al_2Cu are 577, 595 and 548°C, respectively. Moreover, **Table 3** shows the weight percentages of Mg_2Si, Al_2Cu, excess Si and the sum of these three phases. The order of the sums of these phases is those for 6066, 6069, 6082 and 6061 (from high to low). This order is consistent with that for the liquid fraction shown in **Table 3**. These results show that the major phases distributed at globule boundaries are these three phases.

Three main factors affect the generation of fine, uniform, high-liquid fraction and highly spheroidized globular grains in this new type of SIMA process: (1) a proper composition with sufficient elements (e.g., Mg, Si and Cu), which can form low melting point phases for enhancing the liquid fraction, is necessary; (2) the initial extrusion microstructure should be fine and uniform grains for generating fine and uniform spheroidized grains; and (3) particular elements (e.g., Mn, V and Zr) should be added to inhibit grain growth not only to create fine recrystallized grains in the hot extrusion step but also to create fine spheroidized grains in the salt bath step. In this part, 6066 aluminum alloys were the most suitable material for obtaining finest and most spheroidized globules. Therefore, 6066 alloy is used in further researches.

2.4. The parameters of new type SIMA process on microstructure evolution of 6066 aluminum alloy

The influences of salt bath temperatures on microstructural evolution are revealed in **Figure 8**. After salt bath for 30 min at different temperatures, the grains were not spheroidized uniformly

http://dx.doi.org/10.5772/intechopen.70462

as temperature lower than 610°C, and the alloys deformed severely or partially melted as temperature higher than 630°C.

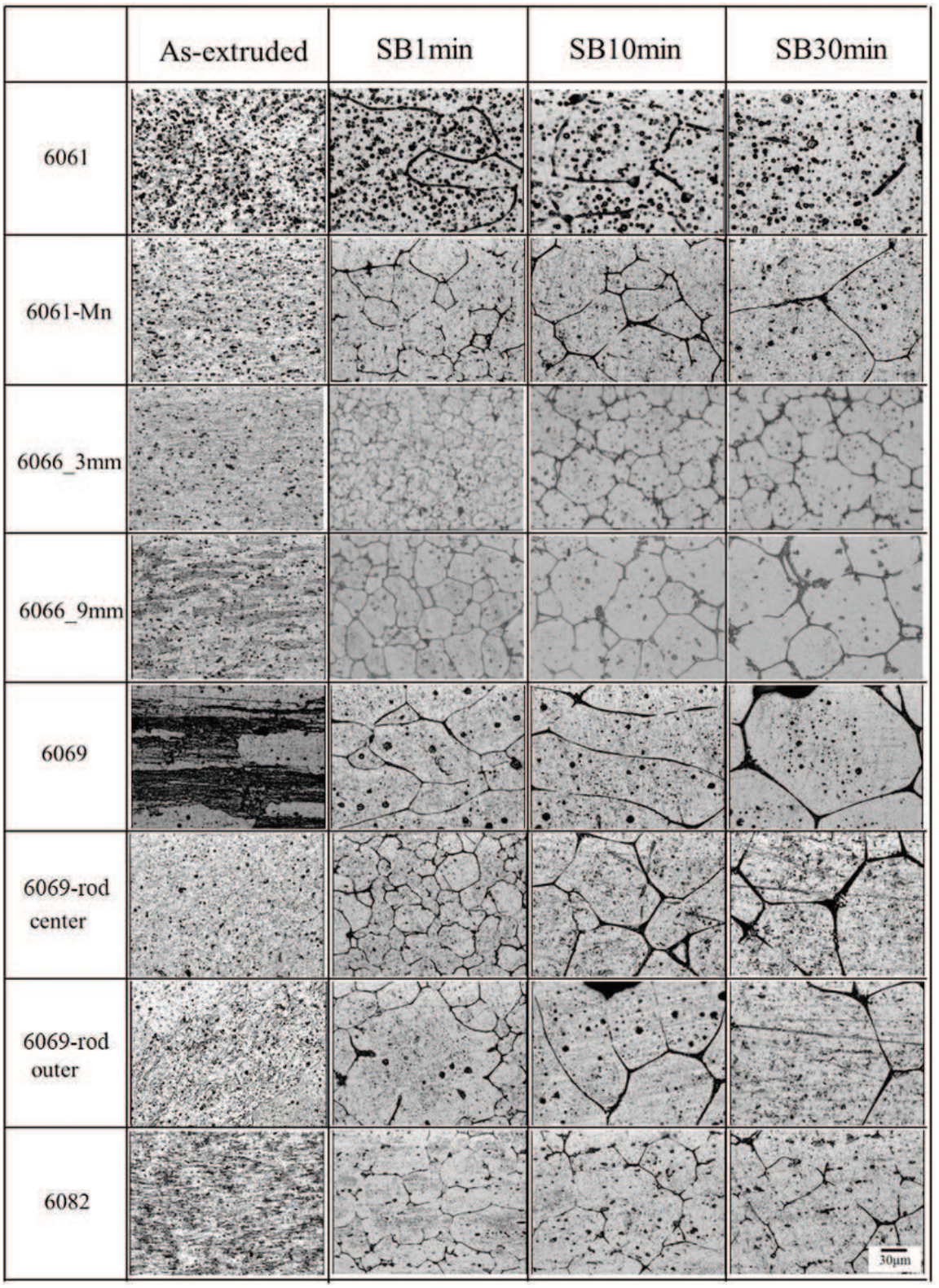

Figure 5. Microstructure evolution of Al-Mg-Si alloys via salt bath.

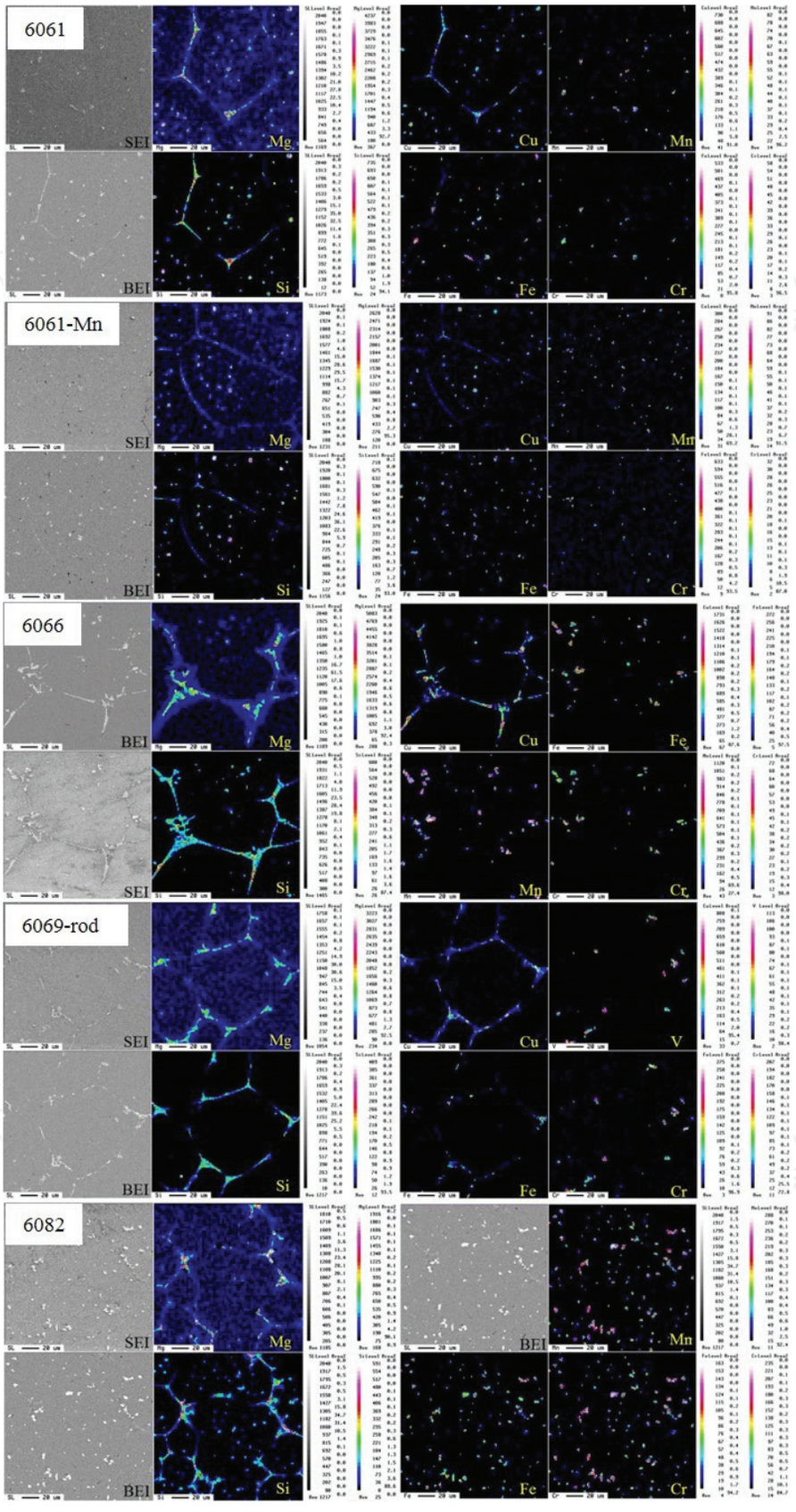

Figure 6. Elementary distribution of Al-Mg-Si alloys.

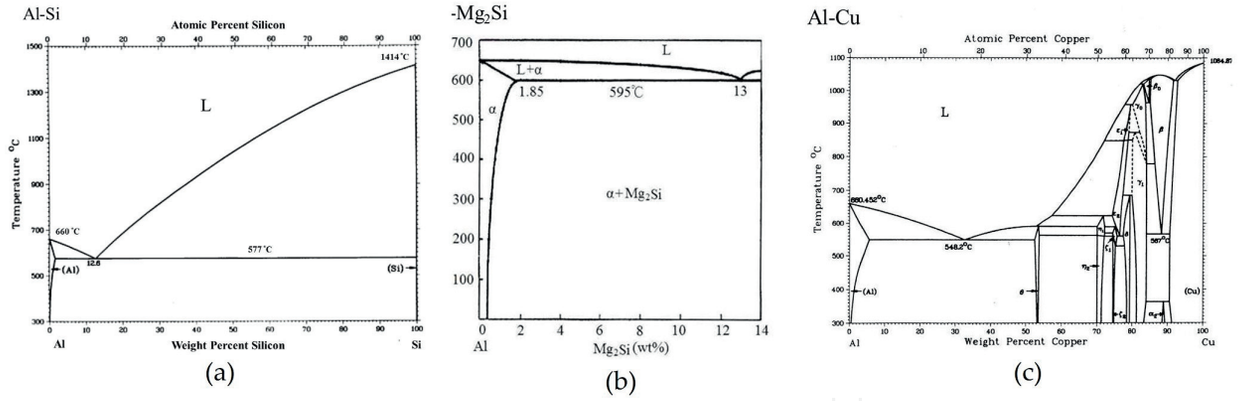

Figure 7. Phase diagrams of (a) Al-Si, (b) Al-Mg_2Si and (c) Al-Cu.

Material	Mg_2Si	Al_2Cu	Excess Si	Sum
6061	1.11	0.33	0.28	1.72
6066	1.61	1.76	0.7	3.97
6069	2.01	1.35	0.07	3.43
6082	1.12	0.11	0.7	1.93

Table 3. The weight ratio of Mg_2Si and Al_2Cu in Al-Mg-Si alloys (wt.%).

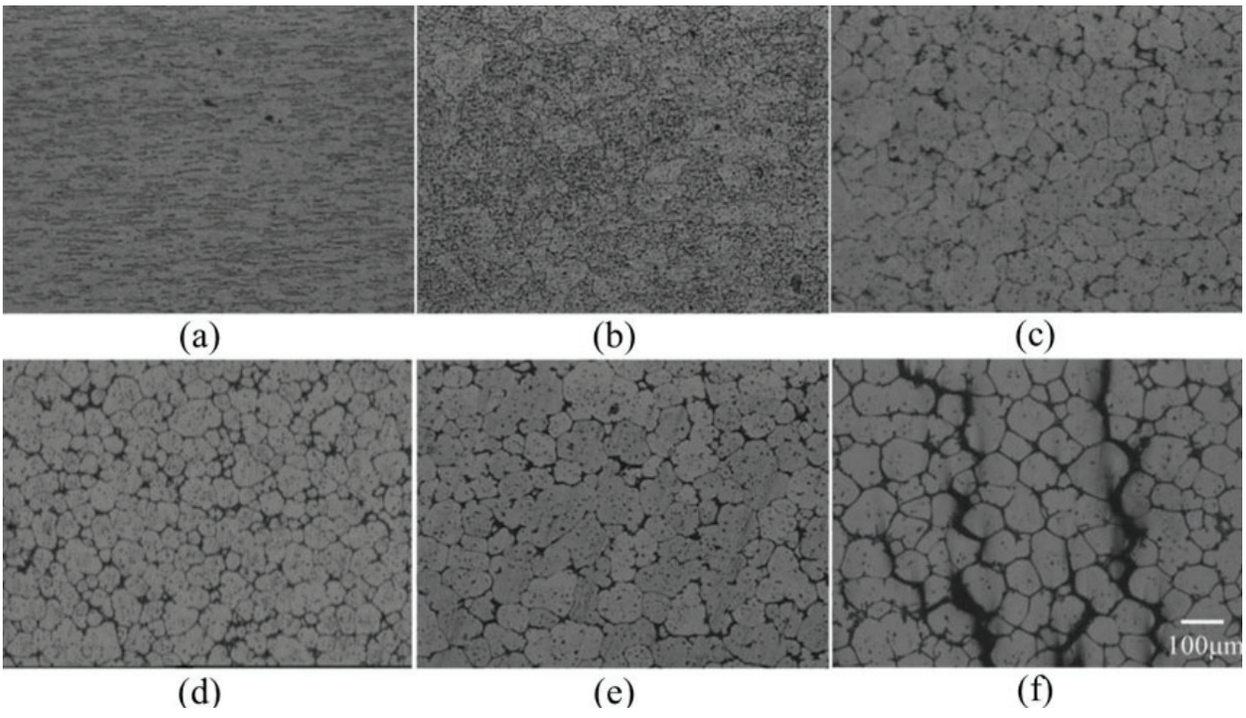

Figure 8. Microstructure of 3 mm-thick 6066 alloy after immersion in salt bath at various temperature and duration: (a) 550°C for 30 min, (b) 570°C for 30 min, (c) 590°C for 30 min, (d) 610°C for 30 min, (e) 620°C for 30 min and (f) 630°C for 7 min.

Figure 9 exhibits the microstructural evolution of 6066 alloys in the salt bath at 610, 620 and 630°C with various duration of salt bath. When salt bath duration increases, the grain growth becomes obvious. A higher salt bath temperature led to higher grain growth for a given period time of salt bath. The grain growth rates for various salt bath temperatures were calculated based on the LSW theory. The linear fitting results are shown in **Table 4**. The results reveal grain growth was very severe at 630°C.

Broadening of globule boundaries was occurred for all temperatures of salt bath, as shown in **Figure 9**. It was resulted from the low melting point phases melting [5–7] and the liquid

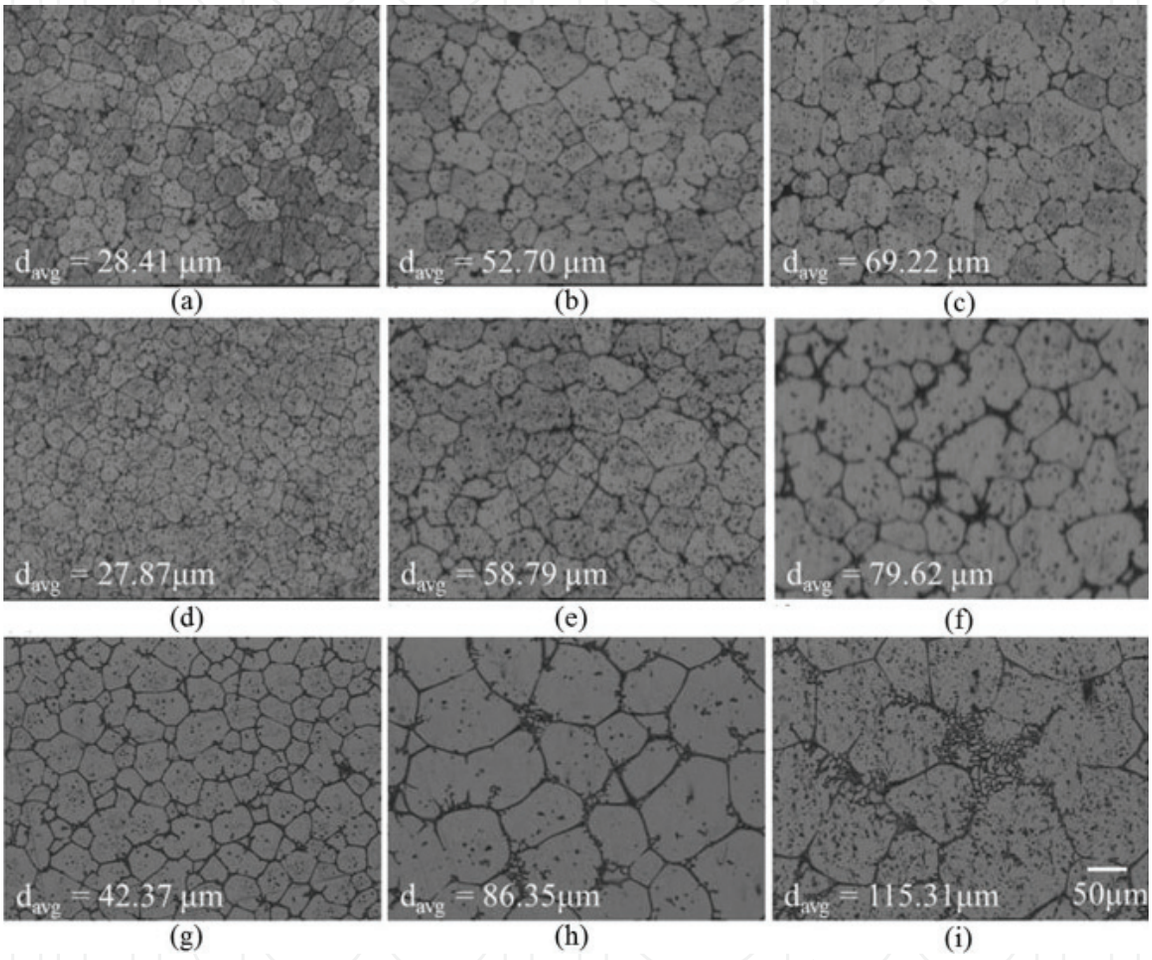

Figure 9. Microstructure evolution with different salt bath conditions of 3 mm-thick 6066 alloy: (a) 610°C for 1 min, (b) 610°C for 10 min, (c) 610°C for 30min, (d) 620°C for 1 min, (e) 620°C for 10 min, (f) 620°C for 30 min, (g) 630°C for 1 min, (h) 630°C for 10 min and (i) 630°C for 30 min.

	6066_3 mm/610°C	**6066_3 mm/620°C**	**6066_3 mm/630°C**
K ($\mu m^3\ min^{-1}$)	10,751	16,806	50,820
R^2	0.9852	0.9926	0.9818

Table 4. K values and coefficients of determination obtained via LSW theory for 6066_3 mm with various salt bath temperature.

http://dx.doi.org/10.5772/intechopen.70462

penetrating the grain boundaries. With the increasing salt bath duration, liquid pools formed due to large amounts of liquid phases aggregating. **Figure 10** shows the liquid fraction. With the increasing salt bath temperature and duration, the liquid fraction increased. Moreover, cracks and voids generated in the materials at 630°C, as shown in **Figure 8(f)**, at which the partial melting occurred and the volume shrank too rapidly during quenching. Even though liquid phase formation at 630°C was the fastest, defects are easily generated. Therefore, the most suitable salt bath temperature was 620°C because liquid formation is sufficiently fast and stable.

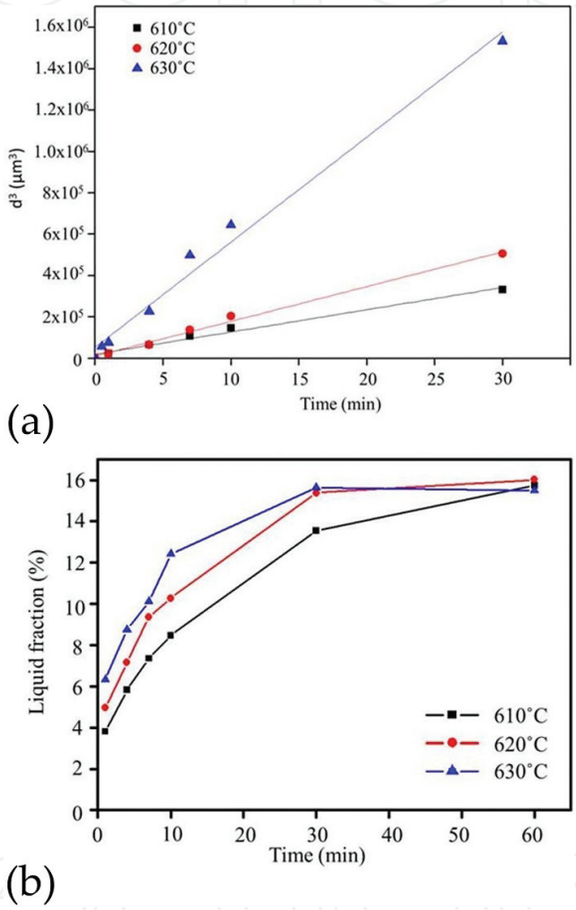

Figure 10. (a) Plot of grain size versus salt bath duration from Lifshitz-Slyozov-Wagner (LSW) theory and (b) liquid fraction for various salt bath temperature (for 3 mm-thick 6066 alloy).

The effect of extrusive ratio on microstructure evolution was discussed by 6066 aluminum alloys with different thickness (6066_3 mm and 6066_9 mm). The microstructure evolution of these two alloys with various salt bath duration at 620°C is exhibited in **Figure 11**. It shows that the average globule size of 6066_9 mm is larger than that of 6066_3 mm at same salt bath duration. High-angle with high free energy grain boundary of recrystallized grains is necessary for SIMA process because they can provide paths for liquid penetrating. However, the amounts of strain introduced by hot extrusion are different in these two alloys with diverse thickness. The recrystallization degree of these two alloys is also different. In 6066_3 mm,

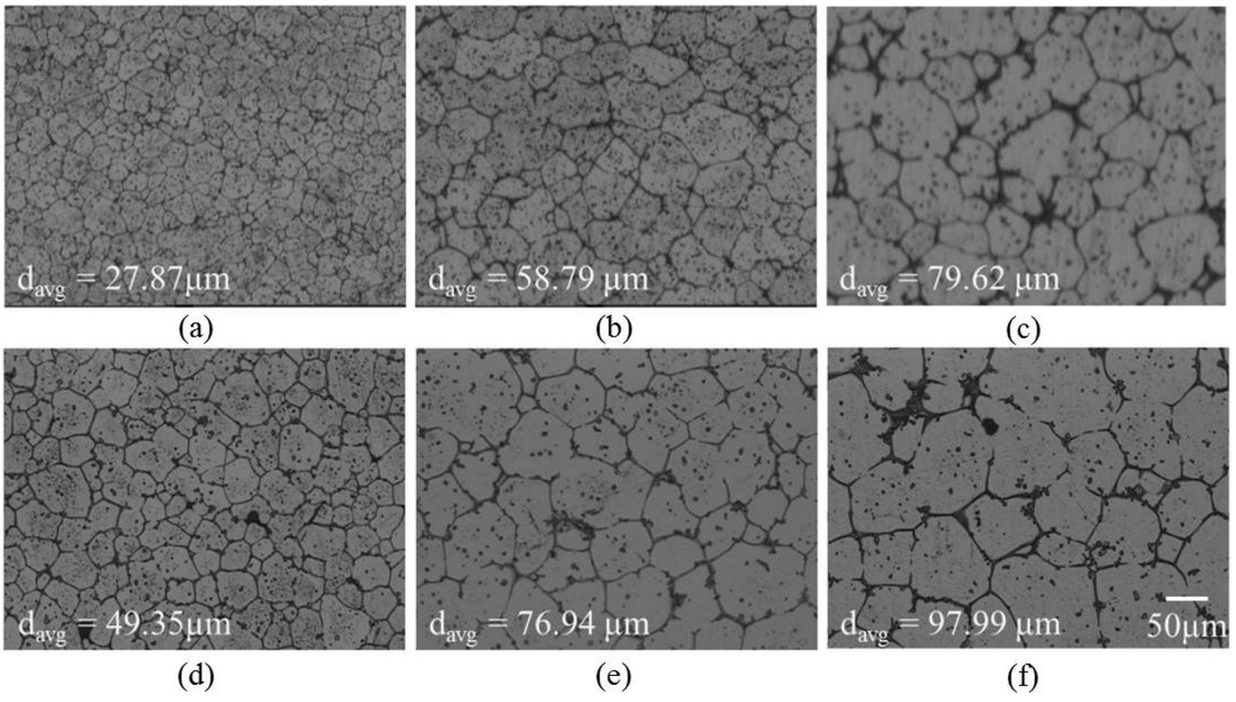

Figure 11. Microstructure of 6066 alloy with two thickness after salt bath at 620°C for various duration: (a) 3 mm-thick and 1 min salt bath, (b) 3 mm-thick and 10 min salt bath, (c) 3 mm-thick and 30 min salt bath, (d) 9 mm-thick and 1 min salt bath, (e) 9 mm-thick and 10 min salt bath and (f) 9 mm-thick and 30 min salt bath.

severe dynamic recrystallization occurred at the hot extrusion step overall the alloys. On the other hand, in 6066_9 mm alloy, dynamic recrystallization occurred only in part of alloy, and static recrystallization also occurred at the step of salt bath. It leads to the different initial recrystallized grain sizes of two as-extruded alloys and also results in different globule size after salt bath. Even though the recrystallization states of these two alloys are different, the grains of those both can be spheroidized.

The relationship between degree of spheroidization and parameters of proposed SIMA process is shown in **Figure 12**. It demonstrates that two shape factors (x and z) are closer to 1 with increasing the duration of salt bath, lower z results from lower temperature of salt bath, and the extrusive ratio do not affect the value of z. These results show that the degree of spheroidization is positive relative to temperature and duration of salt bath but it is not influenced by extrusive ratio. In other words, higher liquid fraction of an alloy leads to higher degree of spheroidization of that.

2.5. Formation mechanism for the two-step strain-induced melt activation (SIMA) process

The mechanisms of globular grain formation for the new type SIMA process are shown in **Figure 13**. The steps are: (1) a suitable composition alloy is cast with uniformly distributed low melting points second phases; (2) disintegrate initial casting microstructure, introduce sufficient strain energy and dynamically grain recrystallize over the alloy through severe hot extrusion; (3) second phases with lower melting points melt and the liquid penetrates grain

http://dx.doi.org/10.5772/intechopen.70462

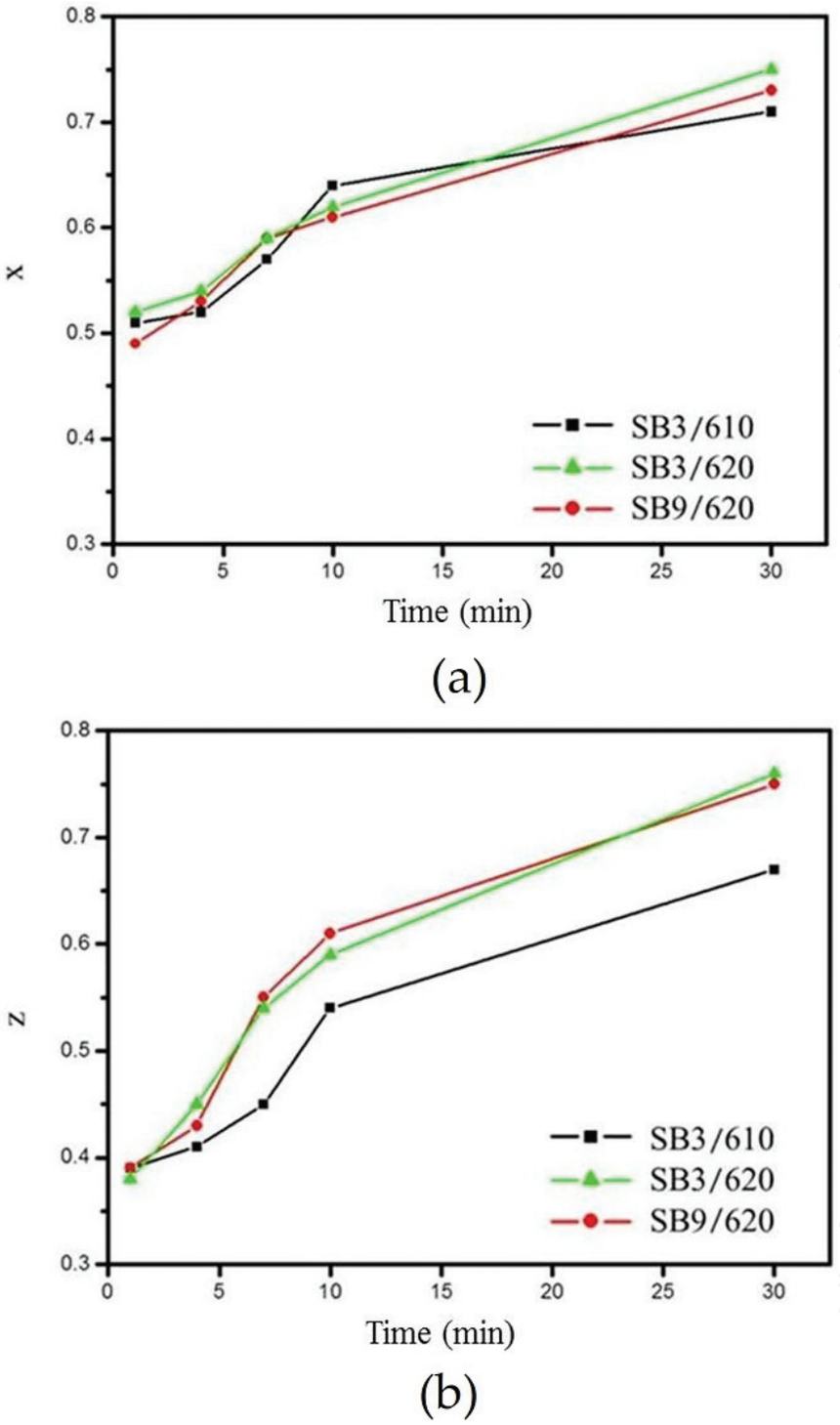

Figure 12. Variation of degree of spheroidization with salt bath conditions: (a) *x* and (b) *z*. SB3: salt bath material with 3 mm thickness; SB9: salt bath material with 9 mm thickness.

boundaries and then surrounds the grains at the step of salt bath and (4) grains grow and become globular with adequate duration of salt bath. This new type SIMA process can produce globular grains faster, and the grains spheroidize uniformly and are finer compared to the traditional SIMA process.

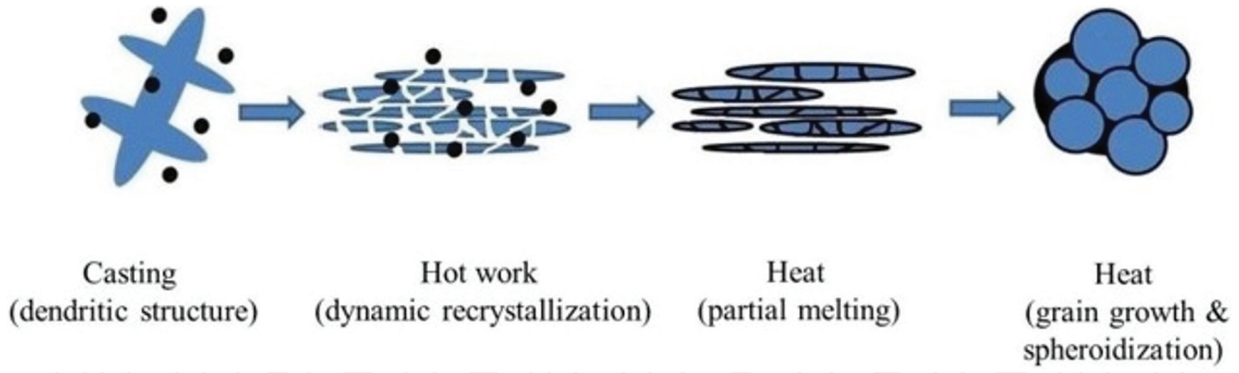

Figure 13. Evolution of globular grain formation in new type SIMA process.

The grains of the 6066_9 mm material can also be spheroidized after the salt bath. It indicates that the static recrystallized grains in the salt bath also provided high-energy grain boundaries for liquid penetration. Both dynamic and static recrystallization can generate grain spheroidization.

2.6. Summary

1. Three major factors to generate fine, uniform, high-liquid fraction and highly spheroidized globular grains in this new type SIMA process: (a) sufficient elements to form low melting point phases, (b) adding some elements to inhibit grain growth and (c) proper extrusive parameters to get fine and uniform initial extrusive microstructure.
2. In 6xxx series alloys, the 6066 aluminum alloy is the most suitable alloys for new type SIMA process. Mg, Si and Cu can generate low melting point phases and Mn can inhibit grain growth.
3. The eutectic phases of Al and Mg_2Si, Al and Al_2Cu and Al and Si are the major phases located on the globule boundaries.

3. High temperature formability and mechanism of deformation of SIMA-processed alloys

3.1. Brief introduction

In this section, mechanical properties and formability under tensile and compressive stress at 500–600°C of the SIMA-processed 6066 alloys were evaluated. And the high temperature deformation mechanism and forming performance were investigated. Besides, the ability of metal flowing and compressibility in a mold of screw at elevated temperatures of SIMA-processed alloys were also estimated.

3.2. Experimental methods

3.2.1. The preparation and codes of specimens

The 6066 alloy is originally a casting column of 6-inch diameter. It was hot extruded in the first step of the new type SIMA process to a 9 mm-thick sheet and to a 3 mm-thick sheet.

Hereafter, "F" will be adopted to abbreviate the hot-extruded sheet material. A 3 mm-thick sheet is used in high temperature tensile test and 9 mm-thick sheet is used in high temperature compressive test, respectively.

In the second step of the new type SIMA process, F was held at 620°C in salt bath (620°C is the best temperature confirmed in Section 2). To vary the size of globule, for different duration, namely 1, 4, 10 and 30 min, were set in this treatment. The specimens of these four different durations will be denoted in the following as S1, S4, S10 and S30, respectively.

Aluminum alloys always manufactured in fully annealed status. The fully annealed alloys will be designated as "O."

3.2.2. Micro-hardness distribution analysis

In order to investigate the difference of hardness between interior globule and globule boundaries, nanoindentation test was performed to evaluate the micro distribution of hardness, using triangular diamond probe with 0.25 nm/s drift velocity and 800 nm depth. The space between adjacent measurement points was 5 μm.

3.2.3. Mechanical test at elevated temperatures and deformation mechanism discussion

A universal material tester was used for the tensile test and compression test. The tensile test was conducted at 500, 550, 600°C and room temperature with the initial strain set at 1.67×10^{-3} s^{-1}. The dimensions of the tensile plate-specimens were shown in **Figure 14(a)**. The broken specimens were used to analyze the fracture mechanism by SEM.

The compression test was performed at 550 and 600°C. Cylindrical specimens with a height of 9 mm and a diameter of 6 mm, as depicted in **Figure 14(b)**, were used. In order to explore the influence of compressive strain rate, two crosshead speeds, namely 3.6 and 36 mm/min, were chosen for the test, which correspond to the initial strain rats of 6.67×10^{-3} s^{-1} and 6.67×10^{-2} s^{-1}, respectively. All specimens were compressed to 70% strain and the flow curves were analyzed to determine flow resistance. The compressed specimens were sectioned longitudinally and subjected to metallographic analysis.

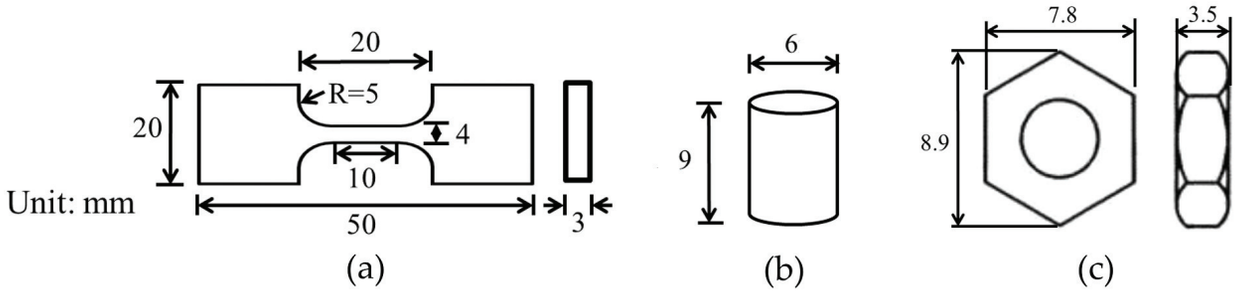

Figure 14. Dimensions of (a) tensile specimen, (b) compressive and forming specimen and (c) screw nut for forming test at high temperature.

3.2.4. High temperature formability evaluation

3.2.4.1. Compression with a given compression rate

In the high temperature compression test with a given compression rate, as-extruded alloys, fully annealed alloys, and SIMA alloys were tested to compare their high temperature formability. The alloys were machined into compression specimens with dimensions of 40 mm (length) × 20 mm (width) × 9 mm (thickness). The compression loading of the dissimilar alloys were measured and compared as 50% compression ratio. The compression ratio is defined as $R\% = (t_0 - t_f)/t_0$, where t_0 is the thickness of the initial sheet (9 mm) and t_f is the thickness after compression. The compression was at 600°C and with 20 mm/min compression rate. The compression resistance is lower as the compression ratio is higher, which indicates that high temperature formability is higher. The compressed specimens were used in further researches of mechanical properties improvement.

3.2.4.2. Forming test at elevated temperature

The high temperature forming test was conducted to 550°C. In the test, cylindrical specimen as those in the compression test was compressed and shaped into a small screw with 0.8 mm pitch. The size of the screw is shown in **Figure 14(c)**. The compressive displacement was set as 6 mm to compare the degree of filling the fringe of different specimens. The crosshead speed was 36 mm/min because the forming efficiency is a great concern in practice. The curves of compressive load versus compressive displacement and the metallographic data of the specimens compressed into screw nut were obtained to determine the resistance of forming, ability of metal flowing and high temperature formability.

3.3. Micro-hardness distribution

The hardness of globule boundaries and liquid pool, where large amount of second phase formed by partial melting aggregated, is twofold to threefold higher than that of the α-Al matrix in grain interior as shown in **Figure 15**.

3.4. Tensile properties of SIMA alloy at different temperatures

Temperatures of tensile test were set at room temperature, 500, 550 and 600°C. F, S10 and S30 were chosen to use in tensile test. **Figure 16** exhibits the breaking features of three materials at room temperature, 500, 550 and 600°C. These figures reveal dimple fracture for extruded alloys, and intergranular fracture for SIMA-processed alloys. Spheroidized grains can be identified on the breaking surface. Quasi-continuous distribution of second phases with low melting point on globule boundaries results in intergranular fracture.

The yield stress (YS) and ultimate tensile stress (UTS) of four materials are below 20 MPa as shown in **Figure 17**. It shows the deformation resistance of 6066 Al alloy is very low at elevated temperatures.

Figure 17 also reveals that the uniform elongation (UE) and total elongation (TE) of F are obviously higher than those of S10 and S30 at all temperatures. The results are due to occurrence of intergranular fracture, which results from quasi-continuous distribution of second

http://dx.doi.org/10.5772/intechopen.70462

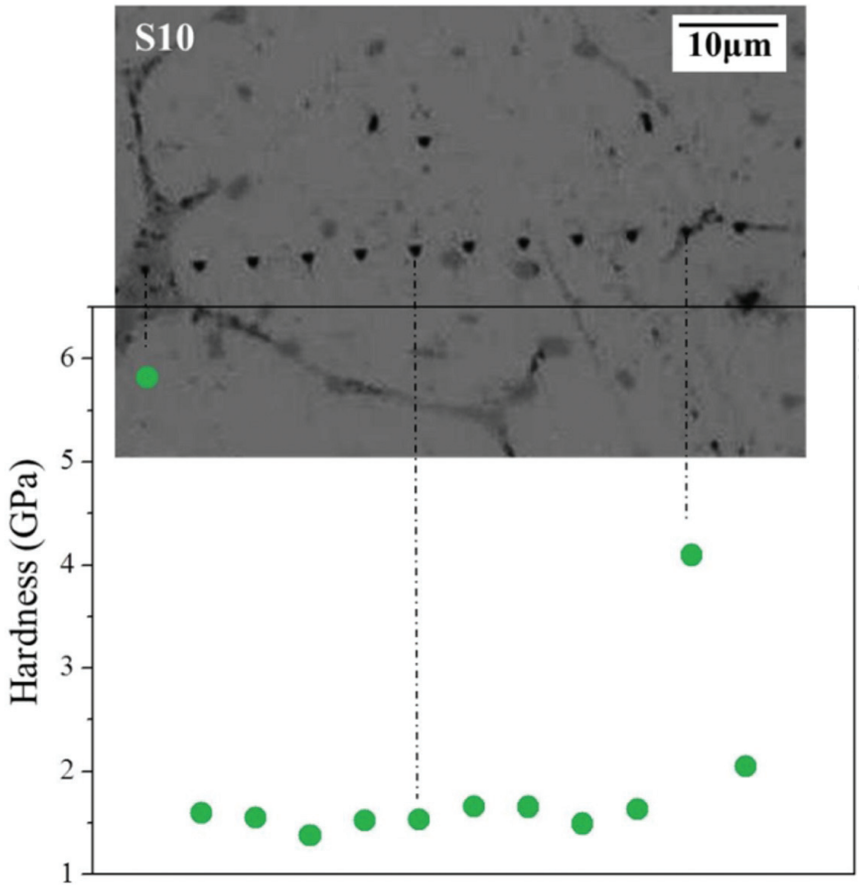

Figure 15. The distribution of hardness evaluated by nanoindentation.

phases with low melting point on globule boundaries. These phases are hard and brittle at room temperature, and they can be softened or partial melted at 500 and 550°C. Therefore, intergranular fracture is the main tensile breaking mechanism of S10 and S30 at room temperature and elevated temperatures. The phases with low melting point on globule boundaries are the weakness when SIMA-processed 6066 Al alloys are subjected to tensile loading at all temperatures. SIMA-processed alloys are not proper for forming with tensile loading.

3.5. Compressive properties and deformation mechanism of SIMA-processed alloys at elevated temperatures

Six materials (F, O, S1, S4, S10 and S30) were compressed at 500, 550 and 600°C to 70% compression ratio with 3.6 mm/min (slow rate, abbreviated as "s") and 36 mm/min (fast rate, abbreviated as "f") in the compression test. No cracks or fractures took place for all materials tested under all conditions as shown in **Figure 18**.

The general tendency of decreasing flow resistance with decreasing compression velocity and increasing temperature as shown in **Figure 19**, which reveals typical flow curves of six materials. The SIMA-processed alloys all had higher flow resistance when they were compressed with slow compression velocity at 500°C. In view of high temperature formability, this result implies poor performance of the SIMA-processed alloy at 500°C.

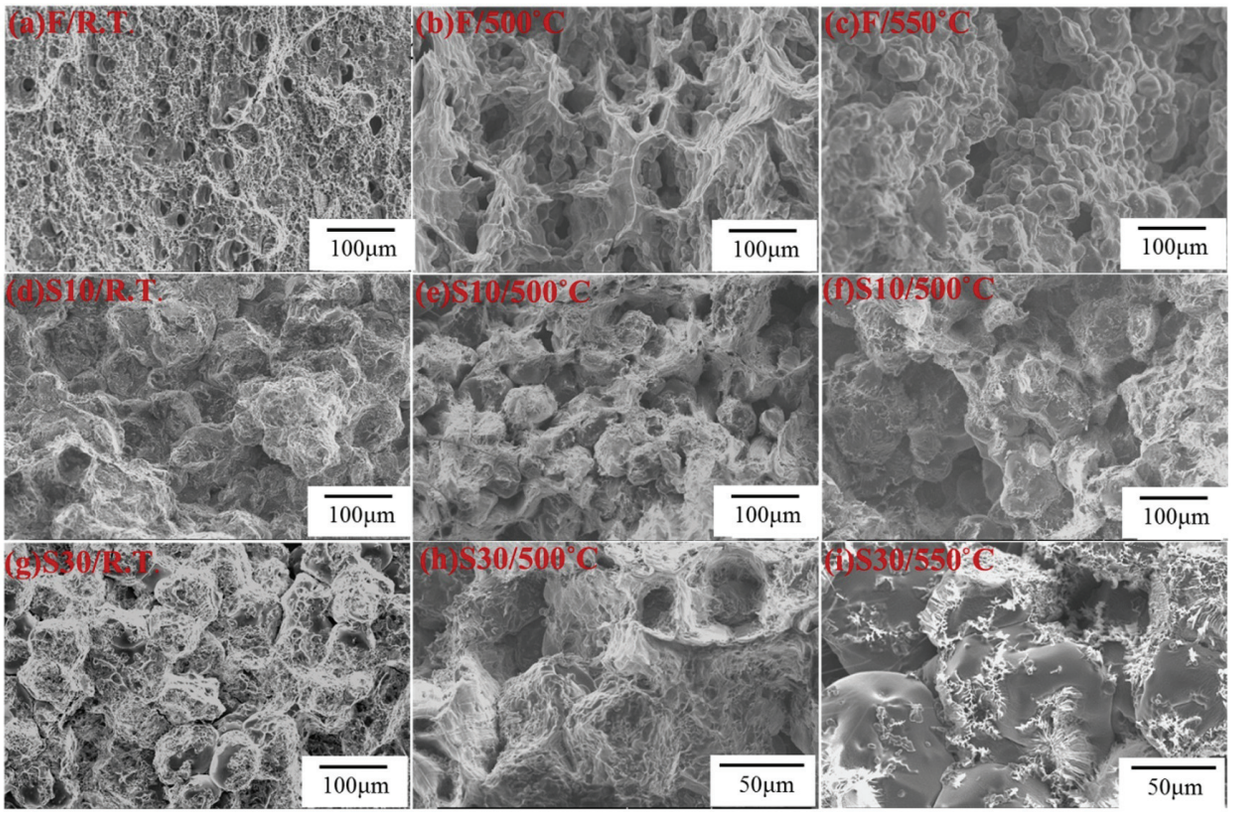

Figure 16. Fracture surfaces of different specimens stretched at various temperatures.

Given in **Figure 19(a)** and **(b)** is the flow curves compressed at 550 and 600°C with 3.6 mm/min. It reveals compression resistance of the SIMA-processed materials are lower than those of F, and they are similar or slightly lower than those of O. Compared to O and F compressed with fast compression rate, **Figure 19(d)** exhibited lower flow resistance of S10 and S30, and **Figure 19(b)** indicates lower flow resistance of S4, S10 and S30. Productivity can be enhanced by a higher compression velocity in practical forming applications. The SIMA-processed alloy compressed at 550 and 600°C with 36 mm/min (fast compression rate) performs low deformation resistance. Therefore, SIMA process is potential to substitute annealing in the pretreatment process of manufacturing at elevated temperatures involving high compression rate.

Figure 20 reveal the metallographic characteristics of the extruded and the SIMA-processed materials of various salt bath durations compressed at 600°C with slow compression velocity. The compressed microstructure of extruded alloy is very uniform, but the compression of the SIMA-processed alloy results in three zones of different microstructure: (1) large deformation zone in center of specimen, in which the spheroidized SIMA grains are severely flattened; (2) free deformation zone near the top and bottom edges of the specimen, in which the spheroidized grains still undeformed; and (3) a transition zone in-between the above two zones. The laminated structure is more distinctive and the globules in free deformation zone become larger when duration of salt bath increased.

Three deformation zones are proposed here and they are formed by the mechanism shown schematically in **Figure 21**. Free deformation zone is generated by globule boundary sliding and flow of liquid, which is formed by low melting point second phases melting. Large

http://dx.doi.org/10.5772/intechopen.70462

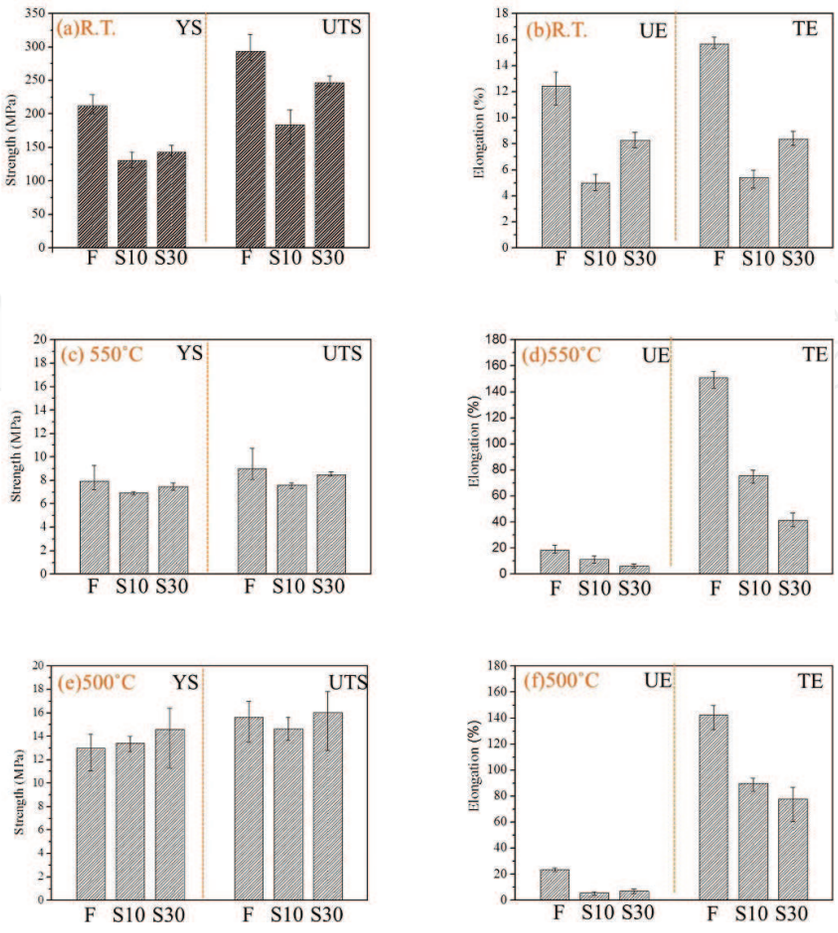

Figure 17. Mechanical properties of F, S10 and S30 at various temperatures (a) strength at room temperature, (b) elongation at room temperature, (c) strength at 550°C, (d) elongation at 550°C, (e) strength at 500°C and (f) elongation at 500°C.

deformation zone is compressed majorly by plastic deformation of the globules, infrequently by flow of liquid and globule boundary sliding. In transition zone, the mechanisms of above two zones co-dominate and compete with each other, hence the microstructure alters with position.

Figure 22 reveals the thickness dissimilarity of the deformation zone of the SIMA alloy for different durations of salt bath. **Figure 22(a)** describes the compression zones and **Figure 22(b)**

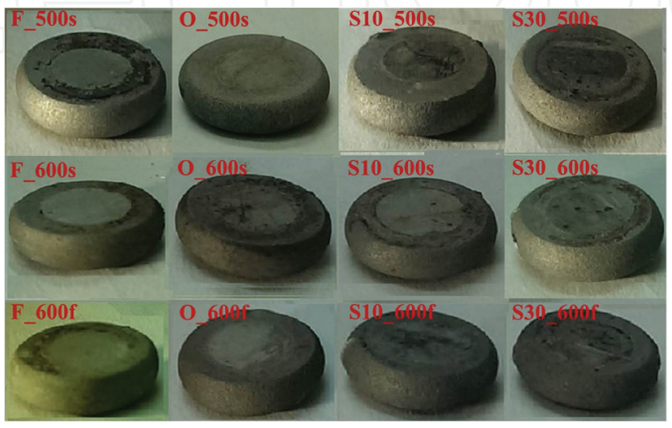

Figure 18. Appearances of several representative specimens.

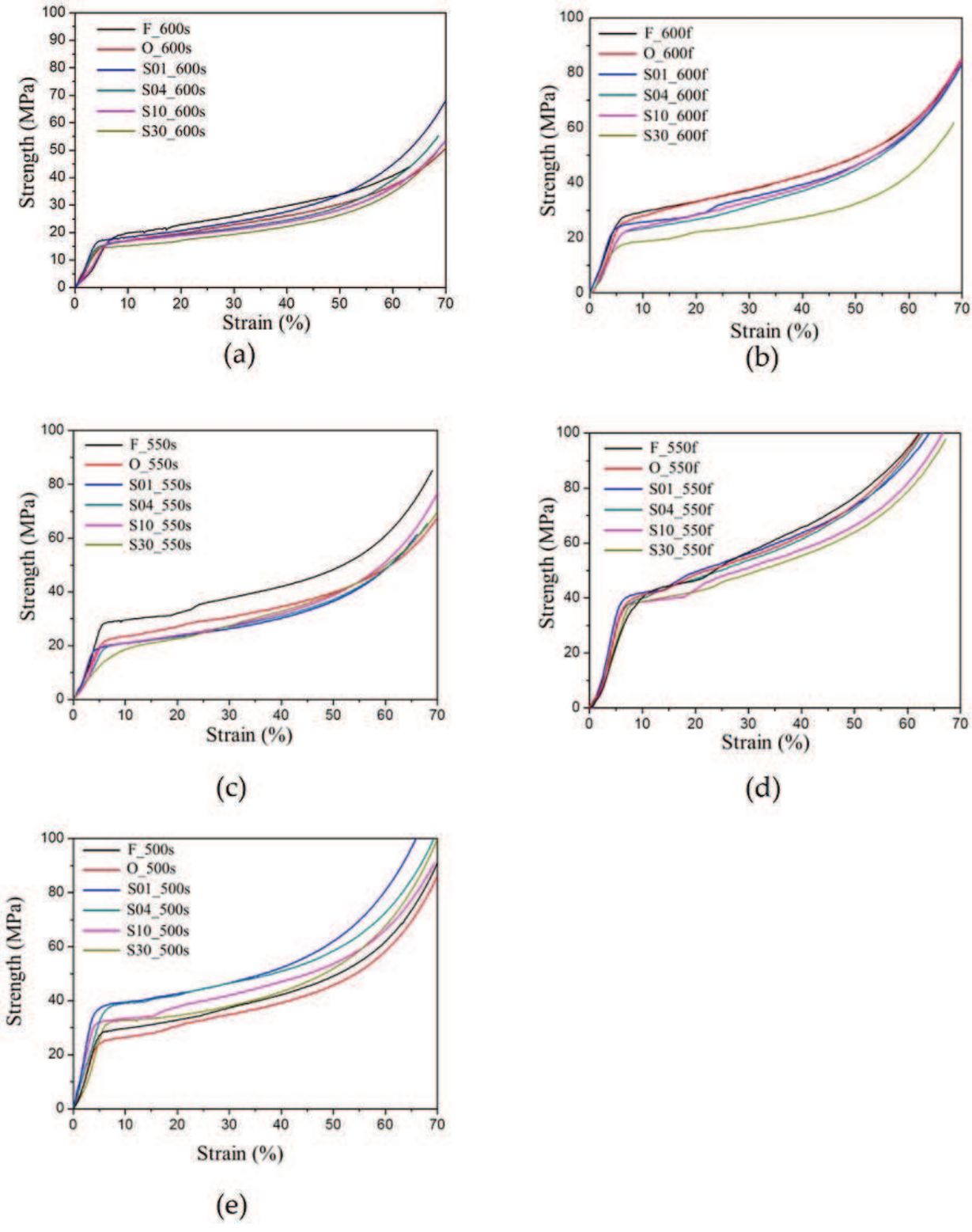

Figure 19. Curves of specimens compressed with different strain rate and at various temperatures: (a) with slow strain rate at 600°C, (b) with fast strain rate at 600°C, (c) with slow strain rate at 550°C, (d) with fast strain rate at 550°C and (e) with slow strain rate at 500°C.

http://dx.doi.org/10.5772/intechopen.70462

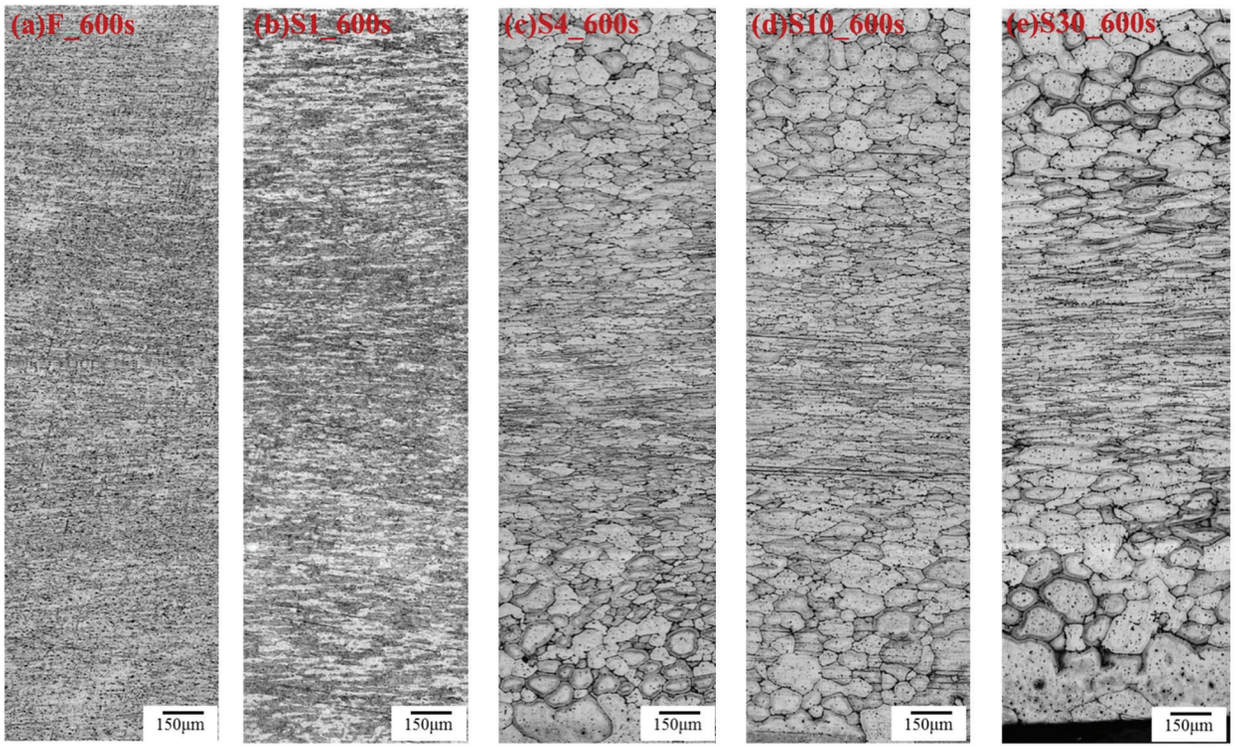

Figure 20. Overall microstructures of various compressing specimens at 600°C.

reveals the thickness of large deformation layer of SIMA alloys. The higher liquid fraction, higher fluidity and more deformed grains at 600°C lead to the thickness was obviously lower than that of 500°C. The thickness of the large deformation layer of the three SIMA-processed materials is close to each other with the slow compression velocity. It is caused by compress stress being decreased by dynamic recrystallization. The thickness of the large deformation layer of S4 is the largest with the fast compression velocity, followed by those of S10 and S30. The reasons are: (1) grain in the large deformation zone (in the center of the samples) limits flowing and sliding of each other, and thus grains deform during compression in this zone. The deformation of small grains (e.g., S4) is more difficult than that of large grains (e.g., S30) [27–29]. (2) The thickness of the large deformation layer decreases with increasing fluidity during compression. The fluidity of the SIMA-processed alloys enhances because of increasing in the fraction of the liquid phases with the salt bath duration increasing.

3.6. High temperature forming behavior of SIMA-processed alloy

3.6.1. Compression test with a given loading

The compression loading at a 50% compression ratio for various materials for the compression at 600°C is shown in **Figure 23**. It shows the compression loading of S10 is the lowest. The new type SIMA process reduced compression loading by about 35% compared with that of the as-extruded alloys, and full annealing reduced that by only about 9%. It indicates that the new

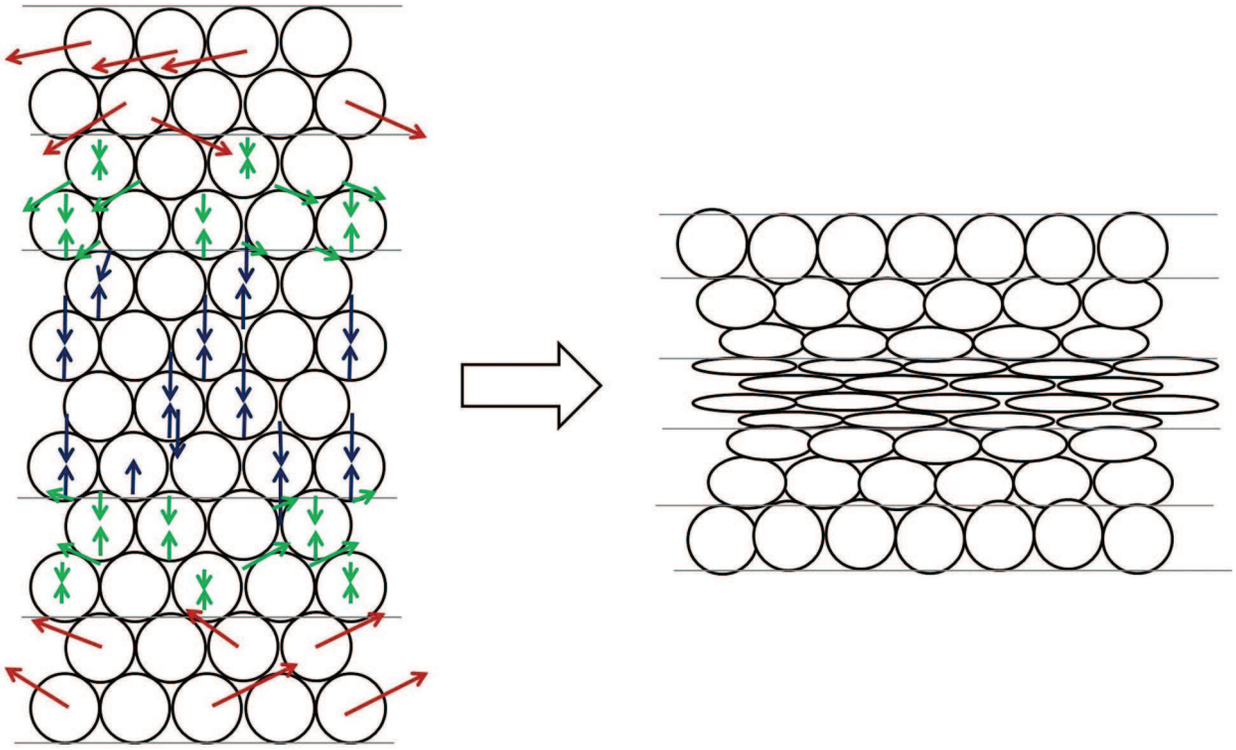

Figure 21. Deformation mechanism of SIMA alloy as compressing.

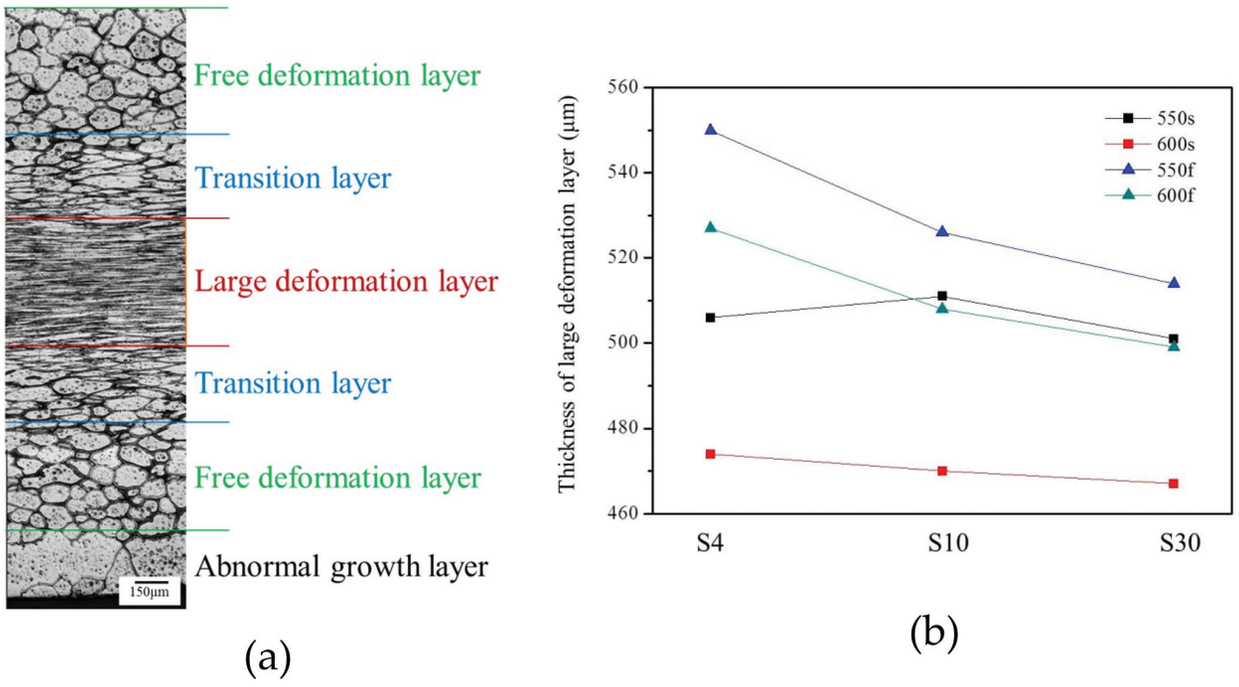

Figure 22. (a) Diagram of compressing microstructure distribution of SIMA alloy and (b) varying trend of large deformation layer with different specimens.

type SIMA process can promote the compressibility at elevated temperatures. The SIMA-processed alloys have the lowest compression resistance.

http://dx.doi.org/10.5772/intechopen.70462

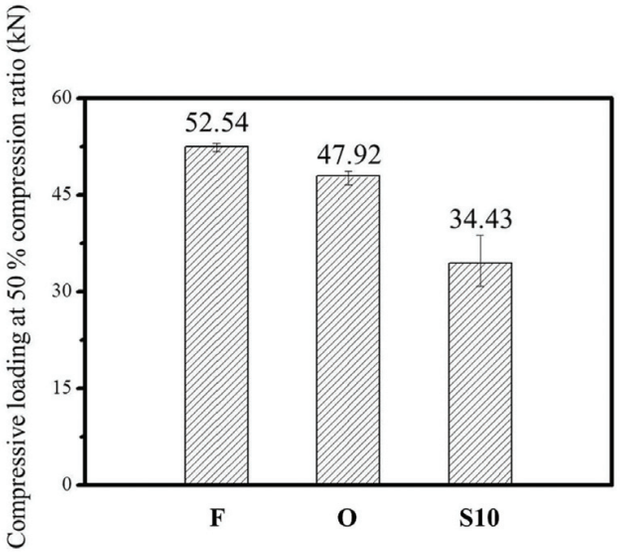

Figure 23. Deformation resistance of several materials.

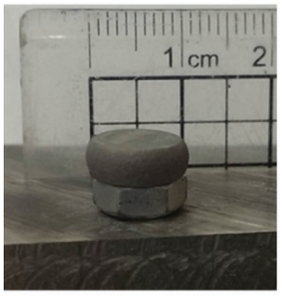

(a)

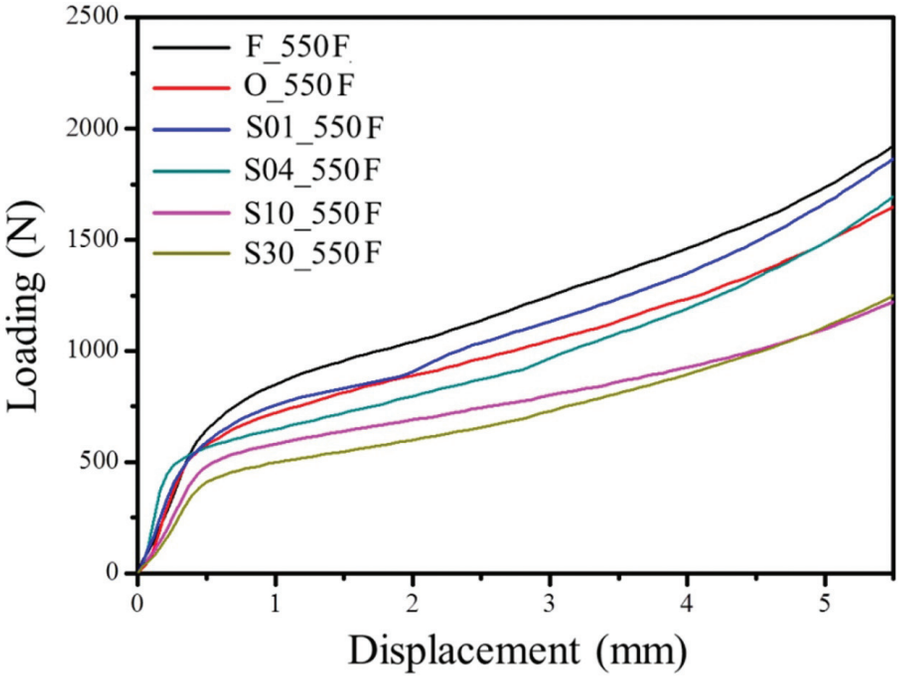

(b)

Figure 24. (a) A photograph of real compressed specimen and (b) curves of specimens compressed with slow strain at 550°C.

3.6.2. Forming test at elevated temperature

F, O, S1, S4, S10 and S30 were compressed and shaped into a small screw nut as shown in **Figure 24(a)**. **Figure 24(b)** shows the order of loading (from small to large) is S30, S10, S4, O, S1

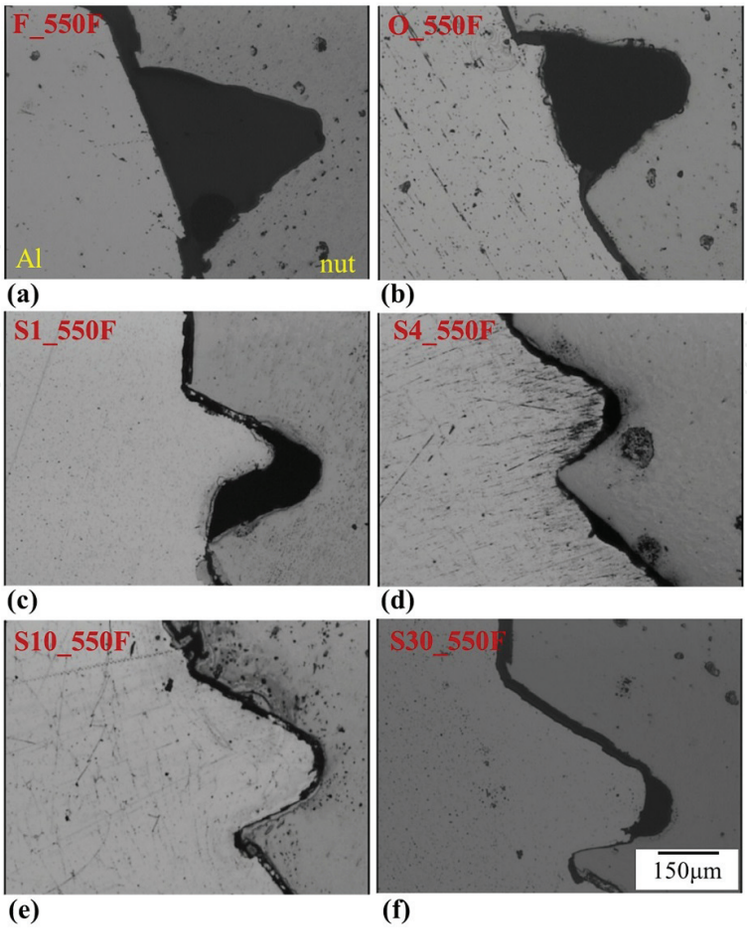

Figure 25. The cross-section microstructures of forming specimens (a) F_550F, (b) O_550F, (c) S1_550F, (d) S4_550F, (e) S10_550F and (f) S30_550F.

and F. The compression loading of S30 is the smallest at any compressive displacement. After salt bath for 4 min, the forming resistance of the SIMA-processed alloy is lower than that of F and O. When salt bath duration is adequate, the forming resistance of the SIMA-processed alloy is relative lower.

Figure 25 shows the microstructure of sectioned-shaped specimens. The position of observation is the first fringe of the screw nut. The degree of filling the fringe (from high to low) is S10, S4, S30, S1, O and F. It indicates S10 has the highest ability of metal flowing. It is due to its suitable globule size and sufficient liquid fraction.

SIMA-processed alloys are suitable for forming with compressive stress. The deformation resistance of the SIMA-processed alloy is low and ability of metal flowing of that is high during compression at elevated temperatures with high compression velocity. The compression formability of SIMA-processed alloys is even higher than that of O. These results prove that the new type SIMA process is applicable for manufacturing with compressive stress. The compression loading can reduce by about 30% and production capability can be enhanced by this SIMA process.

http://dx.doi.org/10.5772/intechopen.70462

3.7. Summary

1. High temperature tensile data show that even though high temperature tensile yield stress of SIMA alloys is small, the elongation and formability cannot compete with F. It is due to the multi-elements and hard grain boundaries melting or softening at high temperatures and generating cracks. Cracks are easy to proceed along grain boundaries and result in intergranular fracture.
2. As compressing temperature is higher than 550°C, the deformation resistance of SIMA alloys descends obviously. With duration of salt bath increasing, deformation resistance decreases more. This advantage is more manifest when compressing rate increases due to dynamic recrystallization appearing as compressing rate being slower. And the results of high temperature forming test prove that sufficient fraction of liquid phase and suitable size of globular grains promotes the fluidity of material and improve the high temperature formability.
3. At high temperatures, the compressive deforming mechanism of SIMA alloy includes two ways: (1) flowing, flow of liquid incorporating solid grains and grain boundary sliding of outer layer of material, which is named free deformation zone; (2) plastic deformation occurring in the center of material due to grains restrict each other to slide and flow, which is named large deformation zone. Between above two zones, transition zone exists. Two mechanisms compete with each other in this zone and result in the microstructure of this zone has gradually variation.
4. S10 is the best one for high temperature forming. It performs low deformation resistance and good fluidity. It proves that suitable size of spheroidized grains is necessary. Notably, intergranular fracture still should be avoided, that is, tensile stress cannot be introduced too much in application.

4. Mechanical properties improvement of SIMA-processed alloys

4.1. Brief introduction

In this section, the improvement of the mechanical properties of SIMA alloys was investigated. The SIMA-processed alloy with 10-min salt bath duration (S10) was used and compared its mechanical properties with that of the as-extruded alloy (F). And the mechanical properties of the SIMA alloy and the as-extruded alloy both strengthened via artificial aging (T6) heat treatment and compared their tensile mechanical properties. Besides, the tensile fracture mechanism of these alloys will be demonstrated.

4.2. Experimental methods

The specimens of tensile test are the compressed specimens with a given compression rate in Section 3.6. It defined as SIMA forming material and marked then with a prefix "C-."

4.2.1. T6 heat treatment and its influences

T6 heat treatment is used for enhancing the mechanical properties. T6 heat treatment includes solution heat treatment and artificial aging. The parameters of solution treatment are set as 530 and 550°C for 2 h, and the parameters of artificial aging is set as 175°C for 8 h (peak aging). Specimens subjected to T6 heat treatment are marked the suffix "/$T6_{530}$" or "/$T6_{550}$." Different solution temperature is used for investigating the effect of amount of solid solution.

4.2.2. Tensile test and tensile fracture mechanism analysis

A universal tester is used in tensile test. Six specimens, namely C-F, C-S10, C-F/$T6_{530}$, C-F/$T6_{550}$, C-S10/$T6_{530}$ and C-S10/$T6_{550}$, were selected to conduct tensile test at room temperature with the initial strain set as 1.67×10^{-3} s^{-1}. The dimension of tensile specimen is shown in **Figure 14(a)**. The tensile direction is parallel to extruded direction.

The tensile fracture mechanism of different specimens was analyzed by tensile sub-surface observing with optical microscope (OM) and fracture characteristic investigating with scanning electron microscope (SEM).

4.3. Mechanical properties improvement of SIMA forming alloys

The tensile properties data of compressed and heat-treated materials are shown in **Figure 26**. **Figure 26(a)** shows the strength data. T6 heat treatment promote the strength of specimens, and the strength of compressed SIMA alloys was slightly lower (by about 10–20 MPa) than that of as-extruded alloys. The ultimate tensile strength (UTS) of SIMA-processed alloys can reach about 430–440 MPa. It proves the strength of SIMA forming alloys after T6 heat treatment is high enough for general applications.

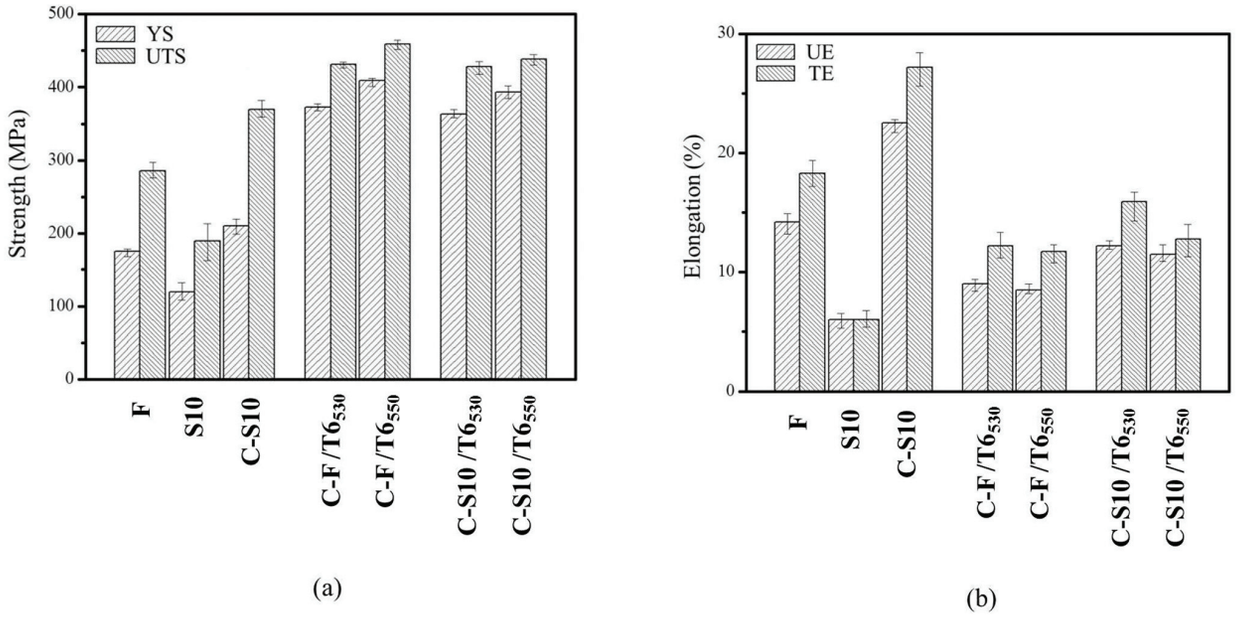

Figure 26. Mechanical properties of specimens: (a) tensile strength and (b) tensile elongation.

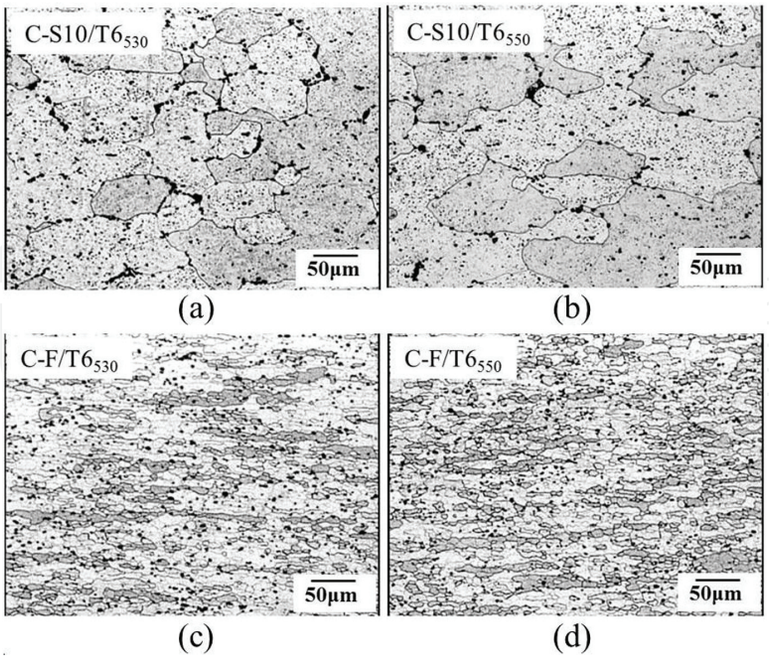

Figure 27. Morphologies of (a) C-S10/$T6_{530}$; (b) C-S10/$T6_{550}$; (c) C-F/$T6_{530}$ and (d) C-F/$T6_{550}$.

The tensile elongation of SIMA-processed alloy is much lower than that of as-extruded alloys as shown in **Figure 26(b)**. Compression at 600°C can enhance the uniform elongation (UE) to about 23% and total elongation (TE) to about 27% because the hard and brittle phases at globule boundaries composed of Al, Mg, Si and Cu diffused into the matrix. Elongation is increased after T6 heat treatment, and it increases with decreasing solution heat treatment temperature. Uniform elongation is about 12% and total elongation is 16% when the solution heat treatment temperature was 530°C. In short, high temperature compression at elevated temperature and T6 heat treatment can improve the mechanical properties of SIMA-processed alloys. An appropriate heat treatment can promote the strength higher than 400 MPa and elongation higher than 10%.

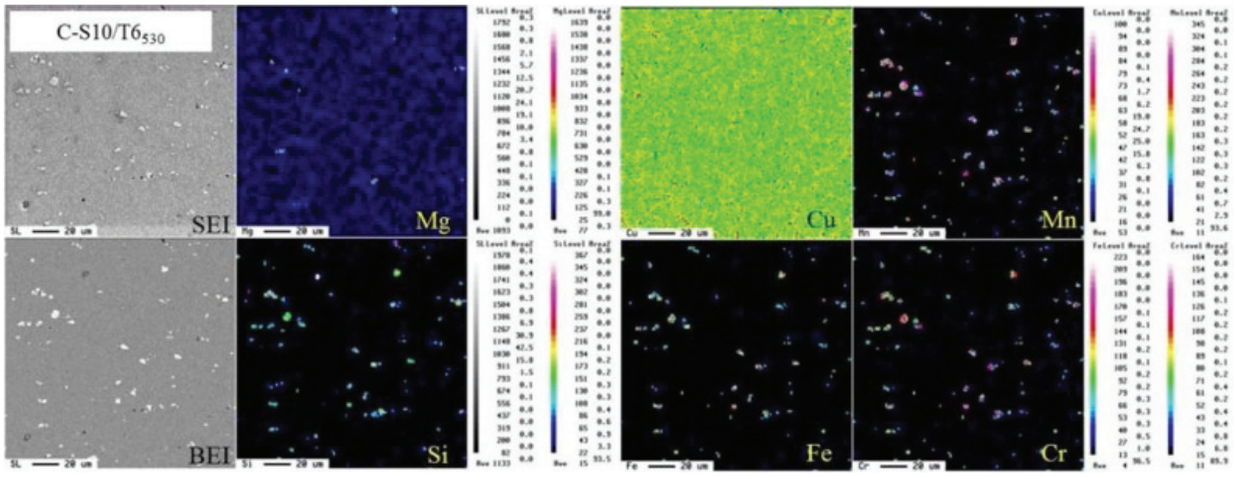

Figure 28. Elemental distribution of compressed TS-SIMA alloy after T6 heat treatment (C-S10/$T6_{530}$) obtained using EPMA.

4.4. Mechanism of tensile fracture of SIMA forming alloys

Figure 27 shows the microstructures of compressed SIMA alloys after T6 heat treatment. It shows that the original compressed globular grains of compressed SIMA alloys grew during solution treatment, as shown in **Figure 27(a)** and **(b)**. The microstructure of T6-heat-treated as-extruded alloys remained as fine recrystallized grains, as show in **Figure 27(c)** and **(d)**. The degree of precipitation strengthening of these two kinds of 6066 Al alloys should be identical

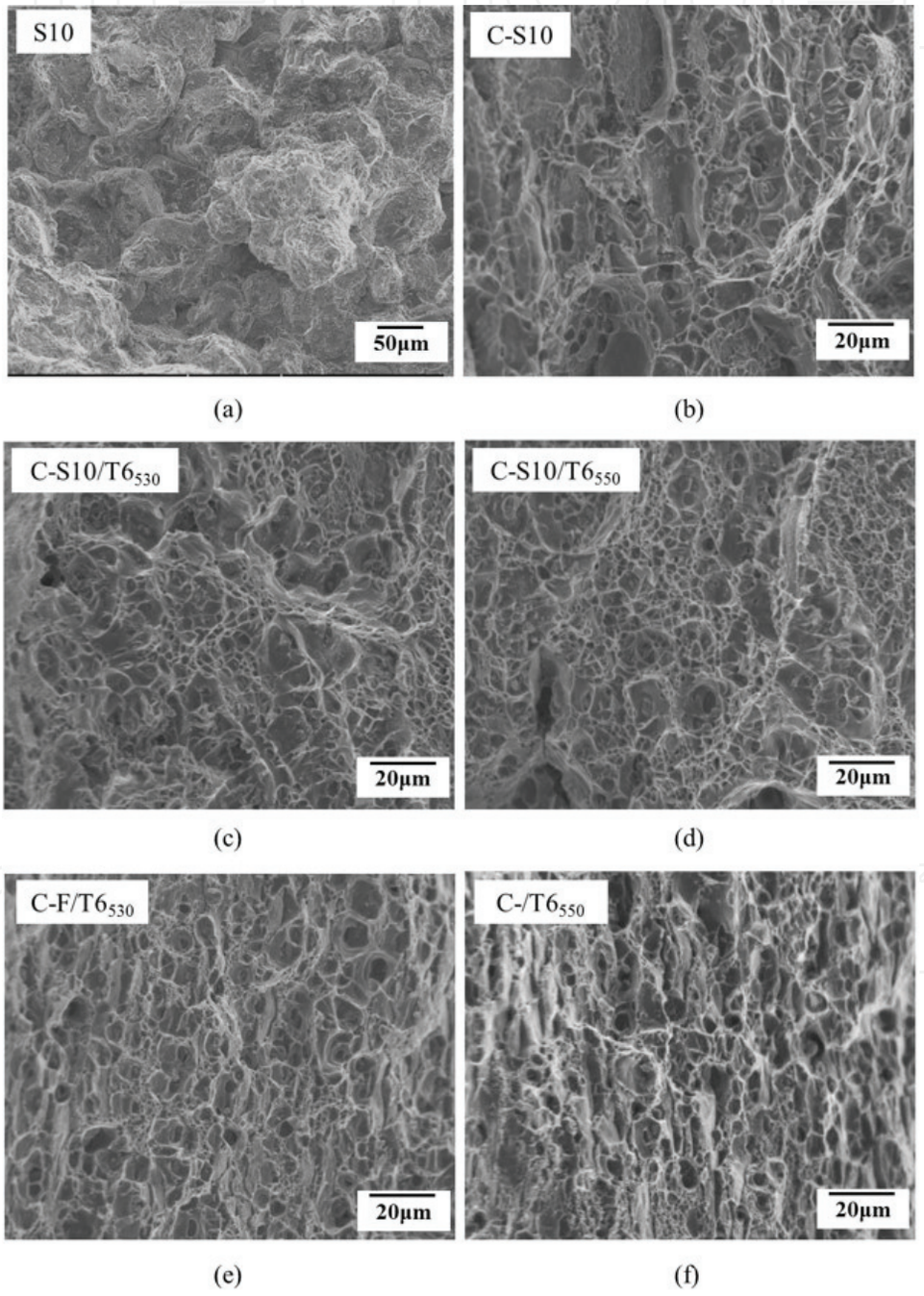

Figure 29. Fracture surfaces of (a) S10; (b) C-S10; (c) C-S10/$T6_{530}$; (d) C-S10/$T6_{550}$; (e) C-F/$T6_{530}$ and (f) C-F/$T6_{550}$.

http://dx.doi.org/10.5772/intechopen.70462

because their compositions and T6 heat treatment conditions are the same. The slight difference of mechanical properties is due to grain size [27–29]. The strength of as-extruded alloys was higher than that of SIMA forming alloys because of the former's fine grains.

Figure 28 reveals the elemental distribution of compressed SIMA alloys after T6 heat treatment. It reveals all elements distribute uniformly. It indicates T6 heat treatment makes Cu, Mg and Si solid-solute and precipitate completely.

Figures 29 and **30** interpret the fracture mechanism of all materials. The intergranular fracture characteristic of SIMA-processed materials is shown in **Figures 29(a)** and **30(a)**. The phases with low melting point melted, penetrated and solidified at globule boundaries, resulting in the globule boundary being more brittle and harder than the matrix. It leads to stress concentration and the generation of cracks. These cracks initiated at globule boundaries and connected with each other, leading to intergranular fracture. Otherwise, **Figure 29(c)–(f)** show the dimple fractures on the fracture surfaces of compressed SIMA alloys and T6-heat-treated compressed SIMA

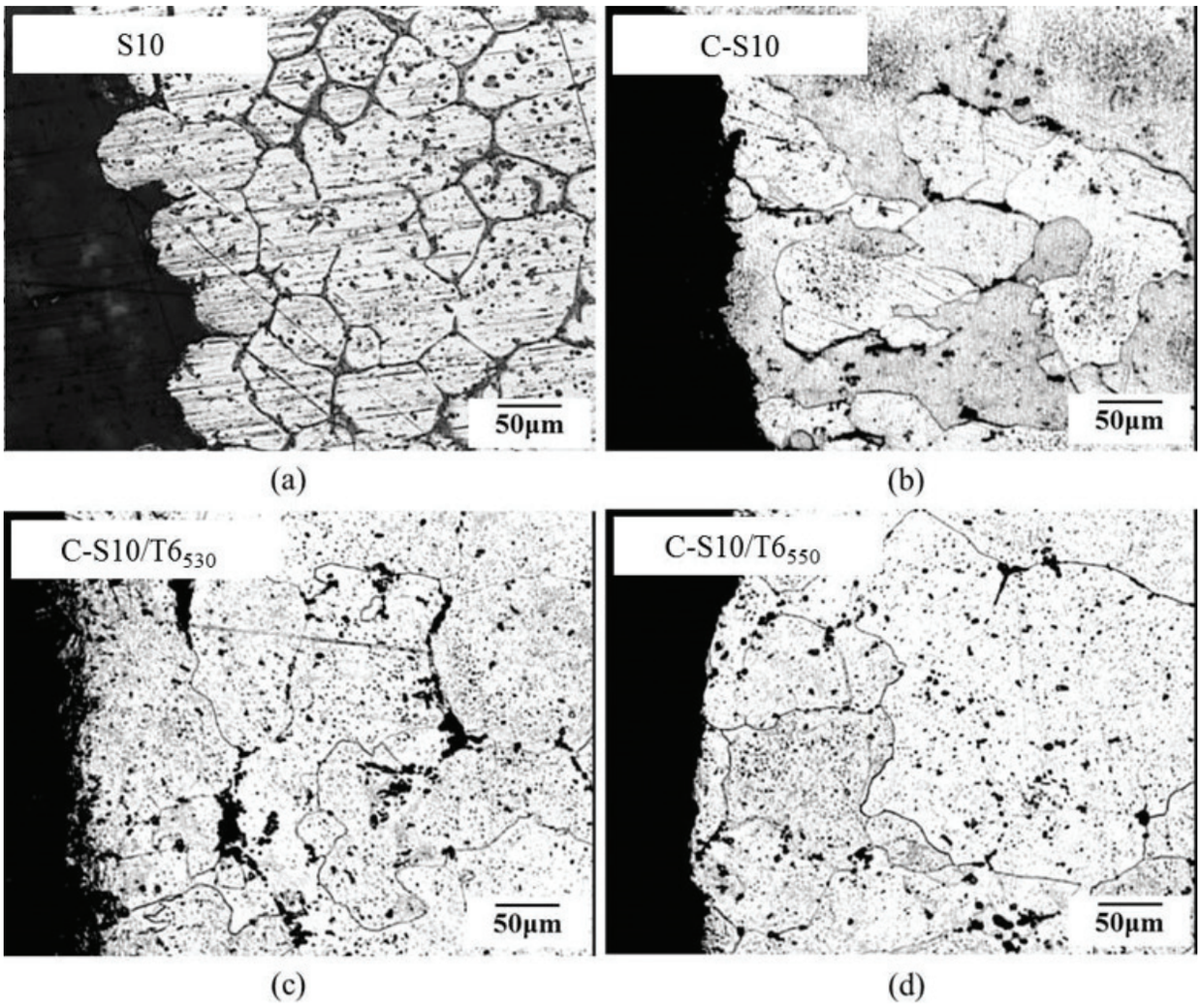

Figure 30. Sub-surfaces of (a) S10; (b) C-S10; (c) C-S10/$T6_{530}$ and (d) C-S10/$T6_{550}$.

alloys. Dimple fracture is a ductile fracture characteristic caused by micro-voids coalescence. **Figure 30(b)-(d)** reveals the sub-surface morphologies of compressed SIMA alloys and T6-heat-treated compressed SIMA alloys. The brittle phases with low melting point disappeared after compression at elevated temperatures, leading to improvement of mechanical properties. After T6 heat treatment, the mechanical properties of SIMA forming alloys are high enough for general applications.

4.5. Summary

1. The mechanical properties of SIMA-processed alloys can be improved obviously (especially elongation) even though that of original SIMA-processed alloys are very low, and T6 heat treatment enhances the mechanical properties of SIMA alloys more to be sufficient for common applications.

2. The improvement of mechanical properties is due to the elimination of brittle and hard phases located on globule boundaries via high temperature compression and solution treatment of T6.

5. Conclusions

1. Three major factors to generate fine, uniform, high-liquid fraction and highly spheroidized globular globules in this new type SIMA process are the following: (a) sufficient elements to form low melting point phases, (b) adding elements for inhibiting grain growth and (c) proper extrusive parameters to get fine and uniform initial extrusive microstructure. For 6xxx Al-Mg-Si alloys, low melting point phases can be composited of Mg, Si, Cu and Al, and globule growth can be inhibited by adding Mn (or V and Zr). Heating method of salt bath results in Ostwald ripening being the major globule growth mechanism. Degree of spheroidization is positive relative to liquid fraction but it is independent on extrusive ratio.

2. At the temperature of solid-liquid coexistence, compressive stress is suitable for SIMA materials forming. Tensile stress will lead to intergranular fracture because brittle and hard phases locate on globule boundaries. Compression of the SIMA-processed alloy results in three zones of different microstructure, namely large deformation zone, free deformation zone and transition zone. SIMA materials perform high compressibility at high compression rate. High spheroidization, high liquid fraction and small globule size enhance the ability of metal flowing and improve the compressibility at elevated temperatures.

3. High temperature compression can improve the elongation of SIMA alloys. The mechanical properties of SIMA alloys can be enhanced by T6 heat treatment. The improvement of mechanical properties is due to the elimination of brittle and hard phases located on globule boundaries via high temperature compression and solution treatment of T6.

Author details

Chia-Wei Lin, Fei-Yi Hung* and Truan-Sheng Lui

*Address all correspondence to: fyhung@mail.ncku.edu.tw

Department of Materials Science and Engineering, National Cheng Kung University, Tainan, Taiwan

References

[1] Wang N, Zhou Z, Lu G. Microstructural evolution of 6061 alloy during isothermal heat treatment. Journal of Materials Science and Technology. 2011;**27**(1):8-14

[2] Fan Z. Semisolid metal processing. International Materials Reviews. 2002;**47**:49-85

[3] Tzimas E, Zavaliangos A. A comparative characterization of near-equiaxed microstructures as produced by spray casting, magnetohydronamic casting and the stress induced, melt activated process. Materials Science and Engineering A. 2000;**289**:217-227

[4] Tzimas E, Zavaliangos A. Evolution of near-equizxed microstructure in the semisolid state. Materials Science and Engineering A. 2000;**289**:228-240

[5] Song YB, Park KT, Hong CP. Recrystallization behavior of 7175 Al alloy during modified strain-induced melt-activation (SIMA) process. Materials Transactions. 2006;**47**:1250-1256

[6] Parshizfard E, Shabestari SG. An investigation on the microstructural evolution and mechanical properties of A380 aluminum alloy during SIMA process. Journal of Alloys and Compounds. 2011;**509**:9654-9658

[7] Paes M, Zoqu EJ. Semi-solid behavior of new Al-Si-Mg alloy for thixoforming. Materials Science and Engineering A. 2005;**406**:63-73

[8] Young KP, Kyonka CP, Courtois JA. United States Patent 4415374. Nov.15 1983

[9] Glickman EE, Nathan M. On the kinetic mechanism of grain boundary wetting in metals. Journal of Applied Physics. 1999;**85**:3185-3191

[10] Zhangm L, Liu YB, Cao ZY, Zhang YF, Zhang QQ. Effects of isothermal process parameters on the microstructure of semisolid AZ91D alloy produced by SIMA. Journal of Materials Processing Technology. 2009;**209**:792-797

[11] Qin QD, Zhao YG, Xiu K, Zhou W, Liang YH. Microstructure evolution of in situ Mg2Si/Al-Si-Cu composite in semisolid remelting process. Materials Science and Engineering A. 2005;**407**:196-200

[12] Ji Z, Hu M, Suguyama S, Yanagimoto J. Formatioin process of AZ31B semi-solid microstructures through strain-induced melt activation method. Materials Characterization. 2008;**59**:905-911

[13] Wang JG, Lu P, Wang HY, Liu JF, Jiang QC. Semisolid microstructure evolution of the predeformed AZ91D alloy during heat treatment. Journal of Alloys and Compounds. 2005;**395**:108-112

[14] Wang Z, Ji Z, Hu M, Xu H. Evolution of the semi-solid microstructure of ADC12 alloy in a modified SIMA process. Materials Characterization. 2011;**62**:925-930

[15] Yan G, Zhao S, Ma S, Shou H. Microstructural evolution of A356.2 alloy prepared by the SIMA process. Materials Characterization. 2012;**69**:45-51

[16] Bolouri A, Shahmiri M, Kang CG. Coarsening of equiaxed microstructure in the semi-solid state of aluminum 7075 alloy through SIMA processing. Journal of Materials Science. 2012;**47**:3544-3553

[17] Hardy SC, Voorhees PW. Ostwald ripening in a system with a high volume fraction of coarsening phase. Metallurgical and Materials Transactions A. 1988;**19**:2713-2721

[18] Atkinson HV, Liu D. Coarsening rate of microstructure in semi-solid aluminum alloys. Transaction of Nonferrous Metals Society of China. 2010;**20**:1672-1676

[19] ASM International Handbook Committee. Properties and Selection: Nonferrous Alloys and Special-Purpose Materials. 1990. p. 51

[20] Hatch JE. Aluminum: Properties and Physical Metallurgy. Ohio: American Society for Metals; 1984. pp. 224-240

[21] Totten GE, Mackenzie DS. Handbook of Aluminum-Physical Metallurgy and Process. New York: Metal Dekker Inc.; 2003. pp. 168-185

[22] Zhen L, Fei WD, Kang SB, Kim HW. Precipitation behavior of Al-Mg-Si alloys with high silicon content. Journal of Materials Science. 1997;**32**:1895

[23] Jeniski Jr RA. Effects of Cr addition on the microstructure and mechanical behavior of 6061-T6 continuously cast and rolled redraw rod. Materials Science and Engineering A. 1997;**237**:52-64

[24] Claves SR, Elias DL, Misiolek WZ. Analysis of the intermetallic phase transformation occurring during homogenization of 6xxx aluminum alloys. Materials Science Forum. 2002;**396**:667-674

[25] Cabibbo M, Evangelista E, Scalabroni C, Bonetti E. A transmission electron microscopy study of the role of Sc+Zr addition to a 6082-T8 alloy subjected to equal channel angular pressing. Materials Science Forum. 2006;**503-504**:841-846

[26] Huang HJ, Cai YH, Cui H, Huang JF, He JP, Zhabg JS. Influence of Mn addition on microstructure and phase formation of spray-deposited Al-25Si-xFe-yMn alloy. Materials Science and Engineering A. 2009;**502**:118-125

[27] Petch NJ. The cleavage strength of polycrystals. Journal of Iron Steel Institute. 1953;**174**: 8-25

[28] Armstrong R, Codd I, Douthwaite RM, Petch NJ. The plastic deformation of polycrystalline aggregates. Philosophical Magazine. 1962;7:45-58

[29] Tilly GP. In: Scott D, editor. Treatise on Materials Science and Technology. 13th ed. New York: Academic Press; 1979. pp. 287-319

IntechOpen

IntechOpen